Chem Soc Rev

REVIEW ARTICLE

View Article Online
View Journal | View Issue



Cite this: *Chem. Soc. Rev.*, 2020, **49**, 1726

# Poly(ionic liquid) composites†

Su-Yun Zhang, ‡[ab] Qiang Zhuang,‡[c] Miao Zhang,[d] Hong Wang,[e] Zhiming Gao,[a] Jian-Ke Sun*[a] and Jiayin Yuan *[d]

Received 26th October 2019

DOI: 10.1039/c8cs00938d

rsc.li/chem-soc-rev

Poly(ionic liquid)s (PILs), as an innovative class of polyelectrolytes, are composed of polymeric backbones with IL species in each repeating unit. The combined merits of the polymers and ILs make them promising materials for composites in materials science. Particularly, the integration of PILs with functional substances (PIL composites) opens up a new dimension in utilizing ionic polymers by offering novel properties and improved functions, which impacts multiple subfields of our chemical society. This review summarizes recent developments of PIL composites with a special emphasis on the preparation techniques that are based on the intrinsic properties of the PILs and the synergistic effects between the PILs and substances of interest for diverse applications.

## 1. Introduction

Poly(ionic liquid)s (PILs), as the polymerization products of an ionic liquid (IL) monomer, have emerged in the last decade as an interdisciplinary topic across multiple research fields, *i.e.*, polymers, ILs and materials science; the wide interest in them is due to their broad range of physicochemical properties and their abundance of chemical structure designs with the use of various IL monomers and backbones.[1–5] Owing to the IL species in its repeating unit, a PIL may exhibit precisely tunable physical and chemical properties, *i.e.*, solubility, ion conductivity (up to $10^{-3}$ S cm$^{-1}$), electrochemical stability (up to 5 V *vs.* $Li^+/Li^0$), thermal stability (300 °C or even higher), and nonflammability,

[a] *School of Chemistry and Chemical Engineering, Beijing Institute of Technology, Beijing, P. R. China. E-mail: jiankesun@bit.edu.cn*
[b] *College of Physics and Optoelectronic Engineering, Shenzhen University, Shenzhen, 518060, P. R. China*
[c] *Department of Applied Chemistry, School of Science, Northwestern Polytechnical University, Xi'an, Shaanxi, 710072, P. R. China*
[d] *Department of Materials and Environmental Chemistry, Stockholm University, 10691 Stockholm, Sweden. E-mail: jiayin.yuan@mmk.su.se*
[e] *Key Laboratory of Functional Polymer Materials (Ministry of Education), Institute of Polymer Chemistry, College of Chemistry, Nankai University, Tianjin, 300071, P. R. China*

† Dedicated to Professor Markus Antonietti on the occasion of his 60th birthday.

‡ These authors contributed equally to this work.

**Jian-Ke Sun**

*Jian-Ke Sun received his PhD degree from the Fujian Institute of Research on the Structure of Matter (FJIRSM), Chinese Academy of Sciences, in 2012. Then he worked as an assistant professor in FJIRSM for one year. After research experience in National Institute of Advanced Industrial Science and Technology (Japan), Max Planck Institute of Colloids and Interfaces (Germany), IBS Center for Soft and Living Matter (South Korea), and Stockholm University (Sweden), he joined Beijing Institute of Technology (BIT) as a full professor in China (2019). He is currently interested in development of ionic porous materials and nanostructured composites.*

**Jiayin Yuan**

*Jiayin Yuan studied chemistry at Shanghai Jiao Tong University (1998–2002), China. He received a MSc degree from Uni. Siegen (Germany) in 2004 and PhD from Uni. Bayreuth (Germany) in 2009. He joined the Max Planck Institute of Colloids and Interfaces in Potsdam as a postdoc and then became a group leader. He received the European Research Council Starting Grant in 2014, Dr Hermann-Schnell Award in 2015, and the Dozentenpreis from the Fund of Chemical Industry in 2016, and became a Wallenberg Academy Fellow in Sweden in 2017. He is from Dec. 2018 a Full Professor at Stockholm University (Sweden). He is interested in functional polymers and carbon materials.*

depending on the type of cation–anion pair, a behavior that is similar to ILs. To integrate their advanced property profile into a variety of applications, PILs can be tailored to compatibly interact with materials of interest through the IL and modern polymer chemistry.[6–10] Reviews of PILs and their material applications have been published by several pioneering groups,[1–6] and they have described a diverse range of topics, including a systematic study of the synthetic strategies, an analysis of the extent of PIL chemical structures, an analysis of physical properties, and a review of their material applications as well as biorelated topics. For example, the synthetic aspects of PILs and the main aspects related to their physicochemical properties (solution and solid-state properties) were reviewed by Mecerreyes in 2011.[4] Our group offered a comparative review of PILs, including synthesis and applications in thermoresponsive materials, carbon materials, and energy harvesting/generation in 2013.[2] In 2017, Yan and Texter *et al.* timely highlighted and updated the novel material applications of PILs over the past few years.[5]

Currently, PILs have dramatically changed the research scope of traditional ionic polymers and polyelectrolytes. This statement can be especially evidenced in terms of their interaction and compatibility with materials actively studied in other fields, such as inorganic materials, metal–organic hybrids and (bio)macromolecules. Controlled integration of PILs and substances of interest may create advanced functional (nano)-composites exhibiting intriguing properties that are absent in or are superior to individual components. Polymer materials have long intrigued many scientific communities, and PIL composite materials are opening up a new dimension in utilizing ionic polymers to offer unique properties and improved functions. To date, PILs have successfully formed many functional composites with metal salts or metal nanostructures, polyoxometalates (POMs), silicas, organic compounds, polymers, metal–organic frameworks (MOFs), carbons (amorphous carbons, graphene, carbon nanotubes), biomaterials, and more.[11–20] Such composites are intensively explored for use in sorption, separation and catalysis processes and in products including batteries, supercapacitors, fuel cells, photovoltaic devices, sensing platforms, and so on.[21–25]

This review will expound this research trend and promote efforts to understand the fundamentals of the role of PILs as an active component for composite design and applications. Furthermore, this review places a particular emphasis on comprehending how to engineer and prepare multifunctional composite materials with advanced functions. In our opinion, this review will inspire and catalyze new research directions to fuel the growth of the PIL material family into a wide range.

## 2. Composite-related properties of PILs

### 2.1 Structural diversity

The properties of PILs can be varied by tuning the structure of the ion-pair composition and/or the polymer backbone. Even when produced from the same IL monomer, PILs can be different when adopting a variety of polymer chain architectures, such as linear, star-shaped, (hyper)branched and cyclic. In addition, an IL monomer can be covalently linked to neutral monomers to form a random, block or grafting copolymer. Given the tremendous array of polymer types, there are unprecedented options in copolymer design. The IL monomer may randomly copolymerize with a common nonionic monomer to dilute the charge character and therefore form a PIL copolymer with an adjustable charge density. In principle, PILs prepared from mechanisms other than traditional (co)polymerization techniques (*e.g.*, free radical polymerization, step-growth polymerization and ring-opening polymerization) can further enrich their structural toolbox. Such diversity in macromolecular design makes the PIL family adaptive to a broad range of composite fabrications.

### 2.2 Adaptive solubility

PIL structures and properties can be modulated readily and uniquely by counterion metathesis, which is experimentally much simpler than restructuring their backbone. In particular, PILs can be shuttled between a hydrophilic and a hydrophobic state through counterion exchange reactions with a foreign salt. For example, by adding a bis(trifluoromethane sulfonyl)imide $(CF_3SO_2)_2N^-$, abbreviated as $TFSI^-$ or hexafluorophosphate ($PF_6^-$)-containing salt into an aqueous solution of a halide-bearing PIL, a thermodynamically driven anion exchange occurs. These anion metathesis reactions allow the PIL to carry $TFSI^-$ or $PF_6^-$ as the counter anion and become hydrophobic enough to precipitate out of its aqueous solution. After separation, it can be dissolved in a targeted organic solvent that may not dissolve the original halide-containing PIL.[26] Such tunable solubility enables a wide scope of processing conditions when crafting composites in polar or nonpolar solvents. A soluble or dispersible PIL in a liquid can electrostatically interact with charged species to associate the PIL with ions, molecules, complexes, polymers, or charged surfaces of insoluble materials, thus laying a foundation for forming composites. These solution mixture systems are compatible with some classical polymer processing methods, such as drop casting, spin coating, electrospinning, and extrusion. Thus, PIL-based composites with well-defined morphologies, such as thin films and long fibers, can be accessed, a feature that is important for specific material applications where distinctive, stable shapes are popular for fabrication and assembly with other components into functional devices.

### 2.3 Chemical stability

Chemical stability is a prerequisite for practical usage. It has been recognized that due to the well-known high stability of IL moieties, PILs can be argued to be more resistant to chemical degradation than most neutral polymers. Nevertheless, side reactions such as structural rearrangement or crosslinking might unexpectedly occur under complex chemical circumstances in a particular device or reaction. For example, the hydroxide anion in PILs might give rise to chemical instability at a high concentration because of its high nucleophilicity.[27] In this context, PILs carrying imidazolium cations might undergo a ring-opening reaction under strongly alkaline conditions at an

elevated temperature. It is common knowledge that the C2-proton in an imidazolium ring or the C3-/C5-protons in a 1,2,4-triazolium ring are active under basic conditions, forming active (poly)-carbene intermediates to further react with other substances.[28]

### 2.4 Thermal stability

Thermal stability defines the operation and processing temperature range of the PIL composites. It is known that the thermal stability of polymers depends on both the repeating units and the backbone. In PILs, the ion pair of the IL unit seems more dominant in defining their thermal stability.[29] Experimentally, PILs depending on the chemical structures of ion pairs and backbones show a wide range of decomposition onset temperatures ($T_{onset}$) that are between 150 and 400 °C.[30] In the PIL $T_{onset}$ database, it is revealed that similar to neutral polymers, the presence of aromatic groups in PIL structures rather than aliphatic groups promotes thermal stability. The thermal stability of PILs decreases with an increasing alkyl spacer length that connects the polymer backbone and the ion-pair component. In terms of cation–anion pairs, the thermal stability of PILs follows the general sequence of imidazolium ~ pyridinium > pyrrolidinium > ammonium for cations and $[Br]^- < [PF_6]^- < [BF_4]^- < [CF_3SO_3]^- < [TFSI]^-$ for anions.[31] Elabd and coworkers investigated the effect of anions on the thermal stability of poly(1-[(2-methacryloyloxy)ethyl]-3-butylimidazolium X) (X ~ anion) and found that the variations in decomposition temperatures for PILs reached ~45 °C. Similarly, Mecerreyes and coworkers tested PILs derived from poly(1-ethyl-3-vinylimidazolium bromide), poly(1-ethyl-4-vinylpyridinium bromide), and poly(methacryloyloxyethyltrimethylammonium chloride). The thermal stability was identified to be in the order of $[CF_3SO_3]^- > [TFSI]^- > [C_{12}H_{25}C_6H_4SO_3]^- > [PF_6]^- > [Br]^- > [C_{16}H_{34}PO_4]^-$.[32]

### 2.5 Tunable ion conductivity

Ion conductivity is a fundamental property of PILs due to their ionic nature. As candidate materials for solid-state electrolytes, PILs attract a broad interest for battery- and fuel cell-related applications. In some cases, a PIL combined with other conductive species could drastically enhance the performance in electrochemical devices.[33] Therefore, understanding PIL ion conductivity is a prerequisite for designing advanced composites for energy devices. After examining the structure of PILs, it is observed that the ion conductivity arises from the motion of counter ions affiliated with the polymer backbone in an electrical field. As most reported PILs are in a solid-state near room temperature, only counter ions behave as charge carriers, while the motion of the ionic backbone is negligible. In other words, PILs are quasi-single-ion conductors. This effect is responsible for PILs having a lower conductivity than their monomeric ILs. For example, the ion conductivity decreased from ~$10^{-2}$ to $10^{-6}$ S cm$^{-1}$ for 1-ethyl-3-vinylimidazolium $TFSI^-$ after polymerization.[34] However, structural diversity in PILs enables tunable ion conductivity. As summarized from recent literature, the ion conductivity of PILs depends on chemical structures, including the backbone, ion pairs,[35] and the spacer between the backbone and ion pairs.[34,36] Elabd and coworkers reported that the ion conductivity increased by over an order of magnitude in copolymers built up from a hexyl methacrylate (HMA) and a methacrylate-based imidazolium IL when the content of the nonionic HMA was increased; that is, the decreased concentration of charge carriers, *i.e.*, the IL density in copolymers, was overcompensated by the lowered glass transition temperature ($T_g$), thus providing increased ion mobility.[37] Bearing a low $T_g$ of −14 °C, poly(1-glycidyl-3-butylimidazolium TFSI) achieved a high ion conductivity of $10^{-5}$ S cm$^{-1}$ at 30 °C.[38] By varying the spacer length between the polymerizable group (the backbone) and the distal imidazolium ring, the ion conductivity can reach $1.37 \times 10^{-4}$ S cm$^{-1}$ at 30 °C.[39] In addition, analogous to hydrophobic ILs, a trace amount of water is readily absorbed into PILs, which facilitates ion transport; this is due to the high-sensitivity of ion conductivity toward the moisture content of the external environment.[40] Such attributes in combination with functional substances may be desirable when fabricating composites for sensors and soft actuators.

### 2.6 Broad electrochemical stability window

PILs bear a part of, if not all, the merits of ILs. Thus, PILs are nonflammable, nonvolatile, and ion-conductive, and they exhibit a wide electrochemical window ranging up to 5.0 V *vs.* $Li^+/Li^0$. This allows PILs to be used as electrolytes for electrochemical operations that are difficult for molecular solvent/electrolyte systems. For pyrrolidinium PILs with $TFSI^-$ as the counter anion, the electrochemical window was reported to be up to 5.0 V *vs.* $Li^+/Li^0$, and this value decreased at high temperatures.[41] Depending on the polymerized ions and semi-free counterions, the electrochemical windows of PILs may be subtly tuned. As mentioned above, the properties of PILs are readily adjustable by the nature of the counterions. Thus, the oxidative-limit sequence of anions, *i.e.*, $[TFSI]^- > [tris(pentafluoroethyl)trifluorophosphate]^- > [TfO]^- > [dicyanamide]^- > [TFA]^-$,[42] for ILs can be a reference for designing electrochemically stable PILs.[43] In addition, a recent study on cations in PILs showed that generally speaking, pyrrolidinium-based PILs currently exhibit the widest electrochemical window.[44]

### 2.7 Universal compatibility

PILs are surface-active materials and are compatible with many materials, including inorganics, organics, inorganic–organic hybrids, and biomaterials. The wide compatibility of PILs toward different substances is ascribed to the noncovalent and covalent bonding categories according to the nature of interactions.

Noncovalent interaction-based hybrids can be assembled through electrostatic interactions, cation–π interactions, hydrogen bonding, and van der Waals interactions. For example, a poly(1-vinyl-3-ethylimidazolium bromide) PIL can transfer CNTs from an aqueous to an organic phase by an anion exchange reaction of $[Br^-]$ with $[TFSI^-]$[45] because of the "cation–π" attractive interaction between the imidazolium cation and the CNT surface.[46,47] Similarly, they can stabilize graphene, which contains

 

π-conjugated aromatic rings,[48,49] and switch the surface properties of the graphene sheets from a hydrophilic to a hydrophobic phase by an anion exchange reaction.[50] In the area of developing electrodes for high-performance supercapacitors, PILs attached to the surface of graphene oxide (GO) enhanced the compatibility of GO with the IL electrolyte to enlarge the effective electrode surface area that was accessible to electrolyte ions; as such, the electrode reached a maximum energy density of 6.5 W h $kg^{-1}$ with a power density of 2.4 kW $kg^{-1}$.[51] The ability to utilize electrostatic interactions is another aspect that can enhance the compatibility of PILs with other substances. By using ion metathesis reactions, functional counterions such as POMs can be introduced into PIL systems. Such electrostatic interactions can even create hybrid materials bearing nanoporous PIL–acid complexes.[52] In addition to electrostatic interactions, PILs also show hydrogen bonding, for example with proton donors such as amino acids.[53]

Covalent binding between PILs and substances is an alternative for composite fabrication. For example, PILs with abundant coordination sites (N, O and P) in their heterocyclic ring can covalently bind to metal substances *via* coordination bonds, leading to the formation of stable composites. Such compatibility with different metal species enables control over the size of nanostructured materials and their morphology.[54,55] In addition, chemical reactions can covalently attach a PIL to different substances. For example, surface-initiated atom transfer radical polymerization (ATRP) enabled a PIL to grow onto a silicon wafer for functional textiles and intelligent microfluidic switching.[56] It is worth noting that covalent hybrid PILs have been generally less studied than noncovalent PIL composites and have high potential for further integration/functionalization; also the noncovalent PIL composites provide a platform for the construction of interesting supramolecular assemblies.[57]

# 3. Synthetic methods

To date, huge efforts have been directed to synthesize PIL-based composites, aiming not only to improve the compatibility of PILs with other components but also to take advantage of the multifunctionality and enhanced properties of PILs for better materials. These composites are widely used in applications of solid-state electrolytes, separation membranes, selective catalysts, sorbents, electrochemical sensors, supercapacitors, and liquid chromatography. As mentioned above, to synergistically combine substances of interest with PILs, the interactions need to be carefully chosen based on chemical structures and physical properties. Typically, the compatible interactions so far reported in the literature of PIL composites can be summarized into two kinds, namely, class I (covalent) and class II (noncovalent), which we have mentioned in Section 2.7. In this review, we classify the fabrication of PIL composites into one-step and multistep methods. Table 1 summarizes the advantages and disadvantages of the typical synthetic methods for PIL composites (Scheme 1).

## 3.1 One-step method

The one-step method is to directly mix a PIL solution with pre-synthesized or commercial substances, including carbons, metal salts, nanocrystals, and organics, *via* covalent/noncovalent interactions. This method involves two approaches: solid–solution mixing and solution–solution mixing.

**3.1.1 Solid–solution mixing.** In a solid–solution mixing approach, PILs and other substances can be mixed, with the former in a solution state and the latter in a solid-state, and *vice versa*. Due to the excellent compatibility of PILs with diverse substances ranging from metals to carbons, PIL solutions are widely used to disperse and modify materials that otherwise easily aggregate in solution, such as CNTs and graphene. For example, CNTs can be added as solid powders and successfully dispersed *via* sonication in a PIL solution without prefunctionalization.[58,59] The association between PILs and CNTs is attributed to a strong π–π/π–cation interaction between the imidazolium cation in PILs and the aromatic CNT surface. Kwang and coworkers mixed a reduced graphene oxide (rGO) powder with an imidazolium PIL-containing solution in propylene carbonate to prepare a rGO–PIL composite *via* both electrostatic and cation–π interactions.[51]

Alternatively, PILs in a crosslinked and insoluble powdered form can be mixed with solutions of substances to prepare composites. This procedure provides good opportunities for importing PIL functionality into the new composites. Dai and coworkers used a series of crosslinked PIL networks (six ion pairs per IL monomer unit) hosting LiTFSI in a solution as quasi-solid electrolytes in lithium-metal batteries. The solid-like polymer electrolytes exhibited an ion conductivity at room temperature of up to $5.3 \times 10^{-3}$ S $cm^{-1}$ by varying the ion

Table 1 Summary of the current methods for the preparation of PIL composites

| Methodology | | Advantages | Disadvantages |
|---|---|---|---|
| One-step | Solid–solution mixing | Direct and easy to perform | Difficult to generate a uniform composite structure |
| | Solution–solution mixing | Easy to perform; a structurally uniform composite; the mixture solution can be further processed into a device, *e.g.*, thin film | Limited to substances that are soluble in solvents |
| Multistep | *In situ* polymerization of an IL monomer in IL-substances | Composites are designable by a judicious choice of IL monomers and polymerization methods | The synthetic procedure is relatively complicated |
| | *In situ* conversion of a substance precursor bound to a PIL | Tailor-made; the (size/spatial) distribution of substances in the composite is well controlled | Complicated synthesis; the PIL should be chemically robust in reaction media during the precursor transformation |

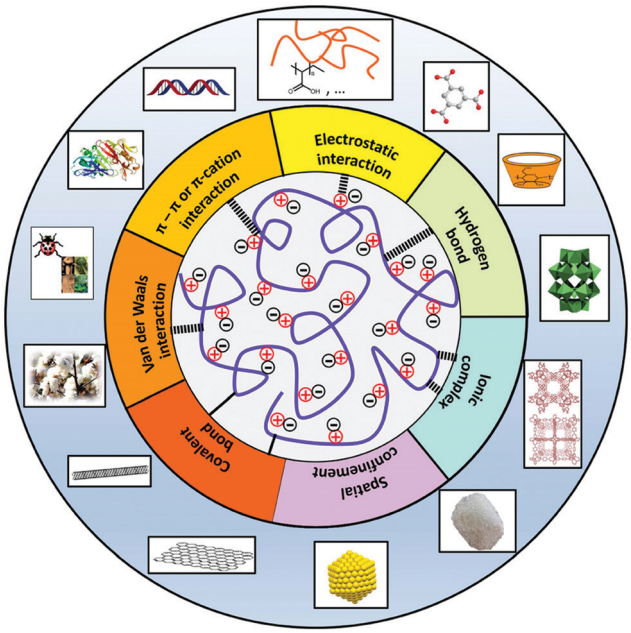


Scheme 1 Various interactions between PILs and substances in composites.

density in the PIL network. Such crosslinked PILs provide abundant, weakly coordinating sites for $Li^+$ transport *via* electrostatic interactions. Moreover, their hierarchical and robust backbone provides the mechanical strength needed in the electrolyte membrane as well as a rich free volume for $Li^+$ motion.[8] In another report, Yan and coworkers doped transition metal salts ($CuCl_2$, $FeCl_3$ and $ZnCl_2$) into a photocrosslinked imidazolium PIL powder *via* coordination interactions to enhance antibacterial activities. The presence of metal ions generated reactive oxygen species (ROS), such as singlet oxygen ($^1O_2$), that progressively oxidized the bacterial cell wall.[60] Yang and coworkers immobilized $Cr^{3+}$ ions onto a $SO_3H$-functionalized solid PIL *via* coordination interactions. Simultaneous functionalization with Brønsted/Lewis acidic groups in such heterogeneous catalysts enhanced catalytic activity.[61]

The solid–solution mixing approach features a facile and feasible way to import the functions of PILs into their composites, such as enhanced dispersibility, ion conductivity, and thermal stability. Nevertheless, only limited examples have been reported so far. In most cases, such heterogeneous solid–solution mixing cannot efficiently generate uniform composites, which may compromise the performance of the fabricated products to some extent.

**3.1.2 Solution–solution mixing.** Considering the limitations associated with the solid–solution mixing approach, a solution–solution mixing strategy is more popular in the fabrication of PIL composites. In solution, both the PILs and other substances appear as free-moving "molecules" or "clusters". Owing to the diverse chemical structures and ionic characteristics in PILs, the substances can be molecularly combined with PILs *via* noncovalent binding, covalent binding or both in solution.

PILs in solution are solvated by solvent molecules and thus are more weakly paired with counterions than when they are in their solid-state. Consequently, it is feasible to incorporate other anionic species into the polymeric skeletons by counterion metathesis reactions. For example, a variety of PIL–POM composites can be prepared by mixing a cationic PIL and an anionic POM aqueous solution due to Coulombic attraction between them. Enhanced photosensitivity in a PIL–POM composite was achieved for use in photocatalysis.[62] More examples of PIL–POM composites are discussed in Section 4.5.

In addition to using ion metathesis, electrostatic interaction is also an effective strategy to produce new functional PIL composites. Our group reported an interpolyelectrolyte complexation method between a cationic hydrophobic PIL and an organic multiacid/polyacid by electrostatic crosslinking in organic solvents.[63] The obtained materials exhibited a nanoporous structure useful in catalysis, sensing and gas sorption.[64] In the long history of polyelectrolyte materials, interpolyelectrolyte complexation in an aqueous phase is dominant. Nevertheless, in the absence of an external inorganic template, such as silica nanoparticles, various attempts to synthesize interpolyelectrolyte complexes have resulted in nonporous or products with pore size far beyond 100 nm. Due to their adaptive solubility, PILs expand the scope of polyelectrolyte complexation from an aqueous to an organic medium. The difference in ionic complexation in water and organic solvents is that the hydrophobic interaction basically diminishes in organic media, and hydrogen bonding can be weakened or canceled as well. Both of them are crucial in shaping the microstructure of the complex products in addition to the Coulombic interaction.

Additionally, weak interactions such as hydrogen bonding and host–guest complexation increase the tools to engineer PIL composites in the solution–solution mixing approach. Charlot and coworkers employed an imidazolium-based IL as the solvent to dissolve guar gum and poly-(1-[2-acryloylethyl]-3-methylimidazolium bromide), which formed a highly conductive ($7.5 \times 10^{-4}$ S cm$^{-1}$ at 30 °C) and elastic ionogel (elastic modulus up to 30 kPa) *via* hydrogen bonds and topologic chain entanglements. The formation of uniform guar/PIL associations in the IL medium enabled a good compromise between the mechanical cohesion and the ion mobility.[65] Ritter and coworkers prepared PIL–organic molecule composites by using cyclodextrin (CD) and poly(1-vinyl-3-butylimidazoloum TFSI).[66] The PIL–CD complex showed pseudo-LCST (lower critical solution temperature) behavior in solution due to the reversible guest–host complexation between CD and $TFSI^-$.

Coordination interactions derived from the functional coordinating sites (N, O, S, and P) in the PIL backbone can drive composite formation in solution, especially for metal or metal complexes. CdSe nanocrystals can coordinate with an imidazolium PIL poly(1-vinyl-3-butylimidazolium $PF_6$) or a PIL-functionalized homolog with a thiol end-group by simply mixing in DMSO.[67] Charge transfer processes may occur between the two components to facilitate the potential integration of PIL into photovoltaic and optoelectronic devices.

In the solution–solution mixing approach, both the PIL and other substances undergo Brownian motion accompanied by a

 

variety of other interactions to drive the formation of the final composites. In this case, PIL composites bearing these interactions can synergistically work with each other, leading to better materials. For example, a PIL-based gel polymer electrolyte was prepared by mixing *N*-ethyl-*N*-methylpyrrolidinium TFSI (P12FSI) and a pyrrolidinium-based PIL and LiTFSI in acetone, which was drop-cast into a membrane.[68] The charged PIL macromolecular structure was associated with ILs and $Li^+$ *via* electrostatic and coordination interactions. This membrane composite was flexible and thermally and electrochemically stable and carried a desirable room temperature ionic conductivity and good interfacial stability with the lithium metal. Schönhoff and coworkers used the same strategy to mix poly(*N*,*N*-diallyl-*N*,*N*-dimethylammonium X) (PDADMA-X, X denotes the anion type) with a Li salt and ILs in DMF to form a gel polymer electrolyte[69] that had improved compatibility and was free of leakage under pressure/vacuum conditions. Similarly, a PIL/IL–Ag composite membrane was obtained by casting a mixture solution of poly(1-butyl-1-methylpyrrolidinium TFSI) (poly[$pyr_{14}$][TFSI]) and AgTFSI, which enhanced the permeability of both $C_2H_4$ and $C_2H_6$ and overcame the hindered gas diffusion in the pristine PIL.[70] The silver salt in the composites boosted the solubility of olefin in the membranes and, upon optimization, enhanced the overall $C_2H_4/C_2H_6$ permselectivity.

### 3.2 Multistep method

A multistep method involves binding the precursor of a substance (substance) to a PIL (IL monomer unit), followed by a chemical reaction to generate PIL composites. In this approach, tailor-made composite structures based on delicate synthetic chemistry can be rationally designed to produce composites with controlled functions and properties.

**3.2.1 *In situ* polymerization of an IL monomer in IL–substance mixtures.** This approach is based on the polymerization of an IL monomer that is bound with substances. Generally, IL monomers are first immobilized on/inside substances such as CNTs, graphene sheets, metal salts, NPs, biomaterials, and organic molecules by an abundance of chemical or physical interactions, followed by *in situ* polymerization to generate PIL chains on/inside substances. An abundance of polymerization techniques, namely, free radical polymerization, ATRP, reversible addition–fragmentation chain transfer polymerization (RAFT), and ring-opening metathesis polymerization (ROMP), can be conducted to introduce task-specific ILs and diverse structures into the final PIL composites.

Polymerization of an IL monomer contained inside hosts is effective to construct PIL composites with prominent synergetic properties due to the possibility of nanoconfinement. For example, Jiang and coworkers integrated imidazolium PILs into the MIL-101 MOF *via in situ* polymerization of encapsulated monomers. The synergistic effects between the good $CO_2$ enrichment and the Lewis acid sites in the PIL and MOF are responsible for the high activity of these PIL composites toward a cycloaddition reaction of $CO_2$ with epoxides; the reaction can form cyclic carbonates at sub-atmospheric pressure. Li and coworkers synthesized a PIL–MOF composite by threading PIL into the UiO-66 MOF *via in situ* polymerization, which exhibited excellent selectivity and fast kinetics for ion exchange, demonstrating that the performance of the composite was better than that of pristine UiO-66 and the commercial anion exchange resin Amberlyst A26.[71] Inspired by the improved performance from the "ship in a bottle" strategy for producing PIL–MOF composites, other nanoporous materials, *e.g.*, COFs and porous membranes, were also utilized as hosts for PIL.[72] Kang and coworkers *in situ* polymerized a 1,4-bis[3-(2-acryloyloxyethyl)-imidazolium-1-yl]butane TFSI monomer in a 1-ethyl-3-methylimidazolium TFSI (EMITFSI)-based electrolyte within a PDADMA–TFSI porous membrane. The well-designed hierarchical composites were used as solid electrolytes and they exhibited superior cycling performance with high specific capacities.[73] Despite limited examples so far, considering the large variety of meso/microporous materials, there are great opportunities to create new PIL composites with complex structures and advanced properties. In particular, polymerization in nanoconfinement can synthesize structure-controlled PILs, which in combination with a porous host may generate myriad properties as a result of structural synergies.

Polymerization of an IL monomer bound to a substance is an alternative for developing PIL composites. In contrast to the above-mentioned porous host, which can only accommodate guests of certain sizes, *i.e.*, the size of the IL monomer must be smaller than the pore size of the host, the current method increases the number of usable substances. Zhang *et al.* developed a series of cyclopropenium–ion hybrid PIL composites by RAFT polymerization.[74] The materials exhibited high ion conductivity and thermal stability owing to the nature of their cationic moieties. Additionally, an IL monomer bearing a catalytically active metallosalen unit can be incorporated by free radical copolymerization into the final PIL–metallosalen composite for heterogeneous catalysts.[75] It is worth noting that the surface-initiated ATRP technique is particularly effective for building PIL chains with a precise length to functionalize a variety of substrates.[76–80] For instance, PIL brush-immobilized mesoporous silica by surface initiated-ATRP exhibited enhanced $CO_2$ adsorption capacity due to the synergy of chemical and physical adsorption by PIL and silica, respectively.[80] By varying the chain length of the grafted polymer on nanosilica, tunable ion conductivity for the hybrid NPs could be achieved.[79] In addition, the PIL brush-functionalized electrode surface, silicon wafer or nanofiber by the ATRP technique can tune surface wettability by exchanging the counteranions of the brushes for those that are more hydrophilic or hydrophobic, which is useful for sensing and electrochemical switching applications.[76–78]

**3.2.2 *In situ* conversion of a substance precursor bound to a PIL.** *In situ* conversion of a substance precursor that is already bound to a PIL is another method for preparing PIL composites. A popular strategy is the chemical reduction of a substance precursor. PIL–rGO and PIL–metal nanoparticles (MNPs) are commonly prepared by this method. Metal salts, including transition metal salts such as $HAuCl_4$, $AgNO_3$, $K_2PtCl_4$, $K_2PdCl_4$, $RuCl_3$, $CoCl_2$, and $RhCl_3$, can be reduced

into MNPs by a reductant such as $NaBH_4$, $N_2H_4$, or $H_2$ gas. Due to the coordination and electrostatic interaction between the heterocyclic cations in the PILs and metal salts, the *in situ* synthesized MNPs can be stabilized by the PILs. The PILs prevent MNP aggregation due to electrostatic repulsion and steric effects. Such PIL–MNP composites are useful as catalysts for olefin hydrogenation reaction, Suzuki coupling reaction, Heck reaction, hydrogen evolution reaction, *etc.*

GO with abundant oxygen-containing functional groups is easily reduced into rGO in an imidazolium PIL solution, which is further dispersed by the PILs and used as an adsorbent for the selective isolation of an acidic protein.[81,82] In particular, the use of conjugated polyfluorene PILs, which are composed of one electron-delocalized planar backbone and two hexyl flexible side chains ending with 1-methylimidazolium bromide moieties, can enhance π–π interactions with rGO sheets; this effect is due to their conductive backbones compared with those of nonconjugated PILs. The PIL sitting on the graphene sheets can prevent their agglomeration during reduction, and the imidazolium bromide ion pair can improve the electrode surface wettability for better electrochemical performance.[83]

In addition to the *in situ* chemical reduction to prepare PIL composites, the *in situ* growth of nano/microsized crystals such as MOFs in PILs based on a coordination-driven scenario is efficient to prepare PIL composites. Li and coworkers prepared a uniform ZIF-8/poly(4-styrene sulfonate) membrane *via* a layer-by-layer method and the use of a coordination-driven self-assembly strategy.[84] Hydrolyzed polyacrylonitrile (PAN)-bound $Zn^{2+}$ was dipped into a $Zn^{2+}$ solution, and a mixed solution of 2-methylimidazole (Hmim) and poly(4-styrene sulfonate sodium salt) was alternatively added to generate a multilayer hybrid membrane. This process significantly suppressed the agglomeration of MOF particles in comparison to the co-blending method, especially at high loadings. Consequently, it exhibited an outstanding capability for removing dye from water, with high retention and good flux observed toward methylene blue far beyond those of previously reported hybrid membranes. Although the *in situ* coordination-driven approach is effective for incorporating nanocrystalline MOFs into PILs, control over the crystal size and MOF composition throughout the composites remains a challenge. Our group developed a coordination replacement protocol relying on a morphological replication procedure that employed a prefabricated ionically crosslinked porous gradient PIL membrane as a reactive template and precursor in a metal ion-containing solution. The kinetics and spatial coupling between the breaking of imidazolium-carboxylate ionic bonds and the immediate formation of Cu-carboxylate coordination bonds produced PIL–MOF (HKUST-1, MOF-74, and Cu-BDC) hybrid membranes with well-grown, dispersed crystals.[57] Moreover, the gradient distribution of the size and mass of the MOF crystals throughout the membrane cross-section from top to bottom was well controlled, which was hard to achieve by the direct co-blending of PIL and MOF particles.

# 4. PIL composites and their applications

## 4.1 PIL–metal nanoparticle composites

MNPs are a subject of global research interest due to their diverse applications in various fields. The stabilization of MNPs is of great concern to avoid their agglomeration during their applications. Employing PILs as stabilizers has gained increasing attention over the past decade due to the following merits: (1) imidazolium/triazolium-type PILs can stabilize most MNPs by associating conventional coordination binding sites in the heterocyclic cations with the *in situ* generated polycarbene structure; (2) PILs as ionic polymers can strongly and selectively interact with oppositely charged species in specific applications; (3) PILs have adaptive solubility that can expand the operation window; and (4) PILs are for the most part chemically and thermally stable and easy to recycle.

**4.1.1 PIL–transition MNP composites.** Transition MNPs have been extensively explored over the past two decades for applications, especially in heterogeneous catalysis. The necessity of nanostructuring the active sites has emerged as a key point in the successful design of catalysts. A PIL with carefully chosen polymeric backbones and ion pairs offers many protocols to immobilize MNPs as nanocatalysts with enhanced activity and selectivity. For example, in 2005, Kou and coworkers used a PIL copolymer poly(1-vinyl-2-pyrrolidone)-*co*-poly(1-vinyl-3-alkylimidazolium halide) to stabilize *in situ* reduced Rh NPs that were 2.9 nm in diameter; the catalyst showed unprecedented lifetime and activity toward arene hydrogenation with a total turnover (TTO) number of 20 000 and a turnover frequency (TOF) of 250 $h^{-1}$.[85] Groppo and coworkers compared the catalytic performance of nonionic imidazole and ionic imidazolium polymer–Pd NP composites. The PIL–immobilized Pd NPs displayed a better chemoselectivity due to the ionic environment provided by the PIL scaffolds.[86] The influence of PIL substituents on catalysis was studied by Lovelock and coworkers. A series of heteroatom donor ($PPh_2$, OMe, $NH_2$, CN, and pyrrolidone)-modified styrenic PILs were used to synthesize PIL–Pd NP composites to catalyze the Suzuki–Miyaura cross-coupling reaction.[87] In particular, the TOF of the optimized system reached 16 300 $h^{-1}$, which was one of the highest reported for Pd NP-catalyzed Suzuki coupling reactions between 4-bromoacetophenone and phenylboronic acid in aqueous media. The ultrasmall size and stability of NPs that was induced by the multicoordination between the PIL and the metal cores, as well as better accessibility to the active metal sites, were responsible for such a high catalytic performance.

Tailor-made nanoreactors with a judicious choice of composition have shown superior performance in accelerating kinetics, enhancing selectivity, and improving the recyclability of catalysts in many traditional organic solvents. A PIL in a micelle-like amphiphilic vesicular shape can form a nanoreactor after being incorporated with MNPs. Recently, we developed a polytriazolium (denoted as P(triaz)) PIL bearing a hexyl substituent, which spontaneously assembled into nanovesicles upon dissolution; additionally, it was capable of

 

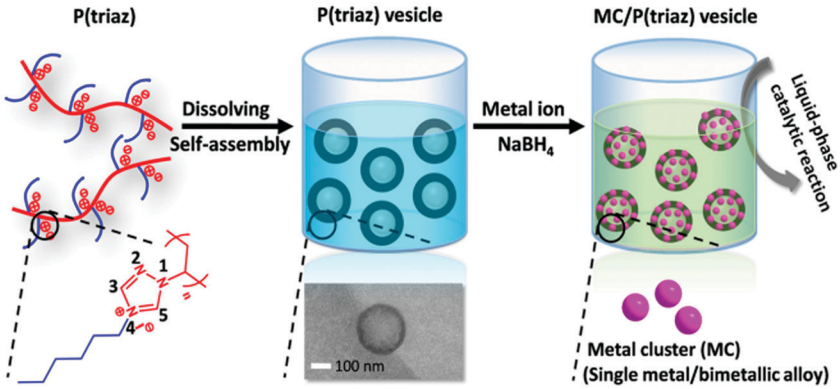


Fig. 1 Synthetic schematic of metal clusters stabilized by structurally well-defined 1,2,4-triazolium P(triaz) vesicles in a dichloromethane and methanol mixture (volume ratio = 2 : 1). Reprinted with permission from ref. 55. Copyright 2017 American Chemical Society.

exerting strict control on the size of metal clusters (MCs), keeping them at ~1 nm (Fig. 1). The association of the traditional binding power of PILs toward metal species with a finely tuned hydrophilicity/hydrophobicity balance and an *in situ* formed poly(N-heterocyclic carbene) (polyNHC) amplified their capping power. An as-synthesized Rh/PIL catalyst exhibited a high activity in a methanolysis reaction of ammonia borane.[55] Furthermore, a hybrid nanoreactor composed of a hydrophobic organic core and a hydrophilic porous silica shell was fabricated from a PIL and mesoporous silica. The Pd NPs encapsulated in such nanoreactors showed significantly enhanced activity and selectivity in the oxidation of primary aromatic alcohols to their corresponding aldehydes in water at a mild temperature (65 °C) and pressure (2 atm). The tailor-made structural design can overcome the common accessibility problem between the substrate and the catalytically active sites; this is due to the unusual solution properties of PILs, which feature a targeted, site-specific enhancement of a hydrophobic substrate in the designed nanoreactor.[88] Alternatively, Dai and coworkers developed crosslinked porous PILs ($S_{BET}$ of 107–132 $m^2\ g^{-1}$) that immobilized Au NPs with an average size of 1–2 nm as a nanoreactor; excellent catalytic activity and selectivity toward aerobic oxidation of saturated alcohol were achieved with a TOF of up to 2064 $h^{-1}$.[89]

To improve the catalytic performance of these hybrid materials, researchers have improved and optimized the chemical composition and molecular arrangements. Compared with bulk reactions, chemical processes performed in microfluidic reactors possess the merits of low consumption of reagents, precise selection of products, and improved energy efficiency; thus, the microfluidic reactors show promise when extending the utilization of supported catalysts from conventional flasks to continuous-flow synthesis. Recently, Zhang and coworkers developed a microfluidic reactor functionalized with Au NP-porous imidazolium PIL composites that exhibited a high conversion activity and selectivity in the reduction of nitrobenzene derivatives; the high catalytic performance stems from improved contact between the substrate and the active sites of Au NPs by surface confinement.[90]

In addition to a one-pot catalytic reaction, the PIL–MNP nanoreactor is also useful in complicated catalytic reactions, such as cascade reactions that benefit from the synergistic effects between the active sites of PILs and metals. For example, a hierarchical organization of PIL–Au NP reactors has been developed as a bifunctional catalyst in which the IL-like units promoted Knoevenagel condensation through a dual electrophilic/nucleophilic activation relay mechanism and the MNPs catalyzed the reduction of the functional groups of the Knoevenagel product in a one-pot tandem reaction (Fig. 2).[91] The structural analysis revealed that appropriately controlling the self-assembly and self-organization of the constitutive building blocks during their synthesis can optimize the microenvironments for each reaction, determining the diffusion of the intermediates from the shell to the core and out from the core to the reaction media.

PILs as effective stabilizers can import "smart" functions such as stimulus-responsive activity, selectivity, and substrate enrichment effects. We developed a fluidic PIL with a low $T_g$ of −57 °C by free radical polymerization of an acrylate-type IL monomer. The synthesized PIL was amphiphilic and acted as a solvent and reaction medium in which highly dispersible and stable Pt NPs with an average size of 3.5 ± 0.4 nm could be obtained in the presence of ethylene glycol as a reducing agent.[92] The as-synthesized Pt NPs were exemplified by

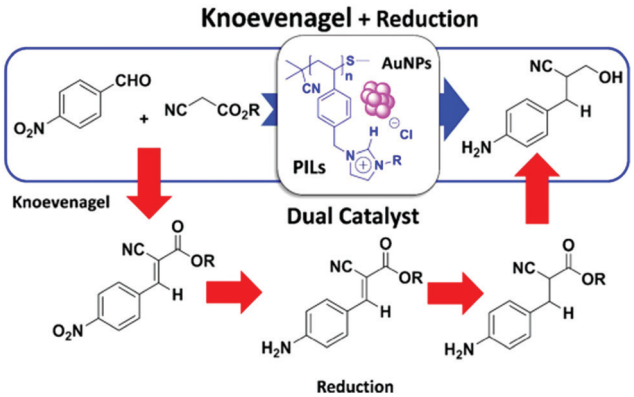


Fig. 2 Dual catalysis based on PIL–Au NP composites for the Knoevenagel/hydrogenation one-pot tandem reaction. Reprinted with permission from ref. 91. Copyright 2016 American Chemical Society.

hydrogenation of the nitroaromatics reaction, in which both hydrophilic and hydrophobic substrates performed well. Such work pointed out the potential application of PIL composites as environmentally friendly, solvent-free and homogeneous fluidic catalysts. Sreedhar and coworkers demonstrated a reversible "solubility switch" of PIL–Ag NPs by an anion metathesis reaction through which the dispersibility of NPs could be easily changed from an aqueous to an organic medium and *vice versa*.[93] The change in the dispersibility of MNPs facilitated MNP-mediated homogeneous and heterogeneous catalysis. Alternatively, Harandi and coworkers prepared a pyridinium PIL copolymer bearing a thermoresponsive block poly(*N*-isopropylacrylamide) (PNIPAM) (denoted as PNIPAM-*b*-PIL).[94] Once incorporated with Pd NPs, such a PIL–Pd composite showed an inherent thermoresponsiveness in C–C coupling reactions that were triggered by the LCST phase transition; above the LCST, the collapsed PNIPAM-*b*-PILs offered a high concentration of substrates around the Pd NPs.

In addition to stimuli-responsive catalysis, PIL–MNP composites can be used as media for stimuli-responsive optical/electronic materials. An example was illustrated in the PIL–Au composite (PIL = poly(1-decyl-3-vinylimidazolium chloride)), in which a lamellar polymer mesostructure was detected in a dried state (Fig. 3). Upon swelling in alcohol, the composite underwent a structural conversion to a disordered state, accompanied by a color change from purple to pale pink and a shift in the surface plasmon resonance to 527 nm, which is consistent with isolated, noninteracting particles. Such a color evolution arose primarily from the synergy of polymer-matrix-assisted changes in the NP packing order and interparticle spacing.[95]

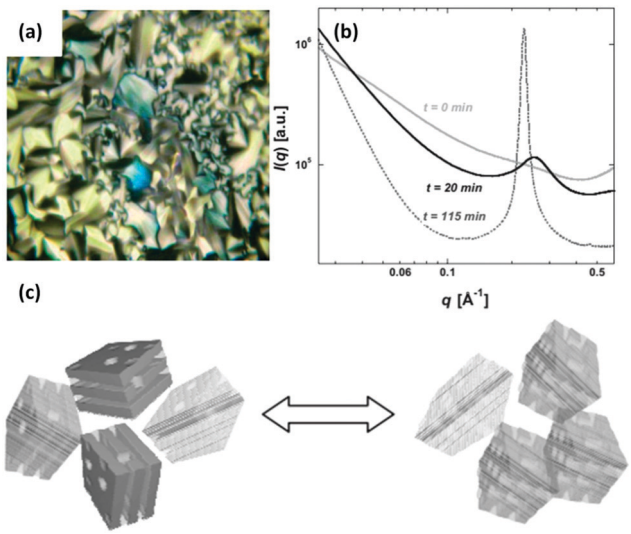


Fig. 3 (a) Polarized optical image (10×) of liquid crystalline textures collected on an *in situ* formed poly[$C_{10}VIm^+$][$Cl^-$] in the presence of a 15 ± 1% (w/w) aqueous $HAuCl_4$ solution. (b) Averaged values of small-angle X-ray scattering (SAXS) data collected at selected time intervals during *in situ* deswelling experiments. (c) Schematic illustration of the structural variation between the mosaic distribution of randomly perforated lamellae and in-plane hexagonal ordering of channels in the lamellae of the polymer composite during solvent evaporation (deswelling). Reprinted with permission from ref. 95. Copyright 2007 Wiley-VCH.

**4.1.2 PIL–metal oxide NP composites.** Metal oxide NPs possessing versatile functions, including magnetism and photoexcitation, are widely used in electronics, catalysis, energy generation, and separation. Many attempts have been made to combine PILs and metal oxide NPs as a composite to achieve synergistic functionalities. Zhu and coworkers reported that PIL/PDA(polydopamine)–$Fe_3O_4$ nanocomposites can quickly remove anionic methylene blue (MB) from water by magnetic collection and be regenerated by washing in a salt solution.[96] Such good performance was benefited by the synergistic effect of the electrostatic interaction (main interaction), hydrogen bonding, and π–π interaction between PIL/PDA and MB, as well as the magnetic NPs for recycling. Similarly, the trimethoxysilane terminated PIL-anchored core–shell $Fe_3O_4$@$SiO_2$ NP composite was explored as an effective adsorbent to extract pesticides from fruits and vegetables,[97] or extract sulfonylurea herbicides from soil.[98]

In addition to magnetic $Fe_3O_4$ NP-based PIL composites, other functional metal oxide NPs, *e.g.*, $V_xO_y$, $TiO_2$, and $La_2O_2CO_3$ with controlled shapes and sizes, have also been utilized as constituent materials for PIL composites.[99,100] Recently, Yan and coworkers reported a PIL composite doped with IL-tethered $TiO_2$ NPs as a gel electrolyte in quasi-solid-state dye-sensitized solar cells (DSSCs). These DSSCs demonstrated improved device performance with an enhanced short circuit current density ($J_{sc}$) and open circuit voltage ($V_{oc}$) compared with DSSCs with unmodified $TiO_2$ NPs (Fig. 4). The effective Grotthuss conduction mechanism enhanced the ionic conductivity and diffusion coefficients of $I_3$ and contributed to improved performance. These results also indicated that the cells based on PIL–$TiO_2$ hybrid electrolytes could overcome the drawbacks of volatile liquid electrolytes and offer a feasible method to fabricate quasi-solid-state DSSCs in future practical applications.[101]

The combination of PILs and MNPs can even generate a composite with functions different from the individual components. For example, poly[(*p*-vinylbenzyl)trimethylammonium $PF_6$]

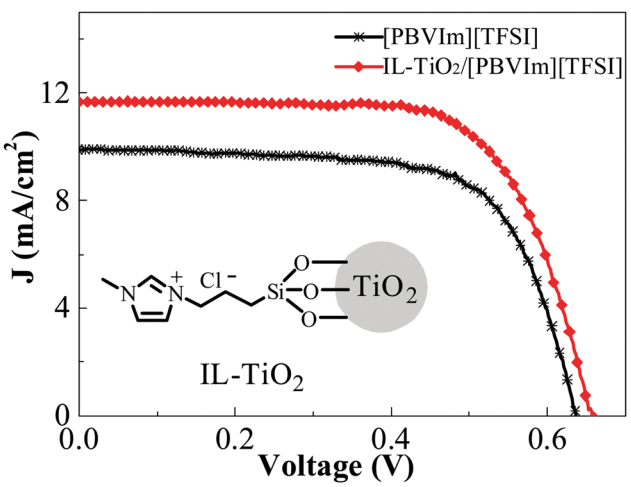


Fig. 4 *J*–*V* curves for the DSSCs assembled with different gel electrolytes under a simulated air mass 1.5 solar spectrum irradiation at 100 mW $cm^{-2}$. Reprinted with permission from ref. 101. Copyright 2012 Elsevier.

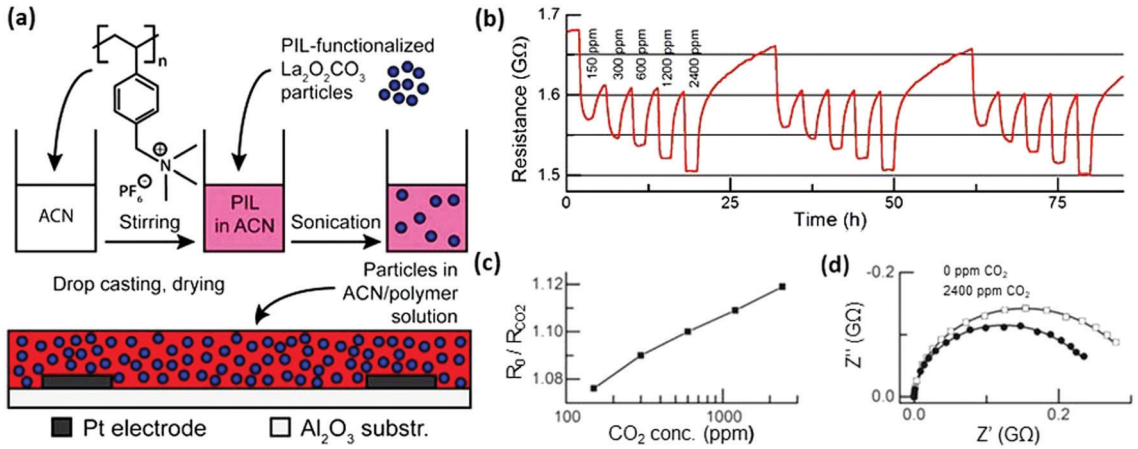


Fig. 5 (a) Sensing performance of thin films composed of 70 wt% $La_2O_2CO_3$ NPs at 50% relative humidity in air and at room temperature. (b) DC resistance change during exposure to $CO_2$ pulses between 150 and 2400 ppm. (c) Corresponding sensor signals, calculated as resistance in air divided by resistance under $CO_2$. (d) Nyquist plots with (circles) and without (squares) 2400 ppm $CO_2$. Measured data (symbols), fitted curve (solid line). Reprinted with permission from ref. 102. Copyright 2015 Wiley-VCH.

and $La_2O_2CO_3$ NPs—both of which are intrinsically insulating materials—were utilized as building blocks to fabricate a composite film by *ex situ* drop-casting on supports. The composite took full advantage of the electrostatic interaction at the interface, which boosted the overall conductivity of the composite at room temperature (Fig. 5). The as-prepared film, with NP loading between 60 and 80 wt%, showed an improved overall conductivity due to the high mobility of $PF_6^-$ anions around the NPs, which was derived from the electrostatic interactions between the cationic PILs and the negatively charged $La_2O_2CO_3$ NPs. The rearrangement of tetraalkylammonium cations in the presence of $CO_2$ was responsible for the enhanced conductivity, which was further demonstrated by an increase in the conductivity when exposed to pulses of $CO_2$ between 150 and 2400 ppm at room temperature and a relative humidity of 50%. The PILs here behaved as a tool to subtly engineer conductive channels localized at the interface by a synergistic interaction between the PILs and NPs.[102]

**4.1.3 PIL–other metal nanostructured composites.** Quantum dots (QDs), an intermediate between bulk semiconductors and discrete atoms, have emerged as promising nanomaterials in applications of transistors, solar cells, LEDs, and sensors due to their size- and shape-determined electronic, optical, magnetic and catalytic properties. QDs are usually suspended in solutions, which are facile for common solution processing techniques such as inkjet printing, spin coating, and Langmuir–Blodgett thin film fabrication. Recently, PILs as a multifunctional dispersing agent have been utilized to bonding QDs for enhanced performance. A PIL hydrogel film incorporated with AuNPs/ZnCdHgSe QD nanocomposites was developed as a photoelectrochemical sensor for the determination of human epididymis protein 4 (HE4) as a diagnostic tool for ovarian cancer.[103] The amino group, the carboxyl group and imidazolium cations within PILs served as attractive sites toward HE4 by hydrogen bonding and electrostatic interaction, and the stable 3D structures facilitated the activity of entrapping proteins for a stable and high-performance sensor. Meanwhile, the AuNPs/ZnCdHgSe QDs act as cooperative photoactive elements to create an enhanced photoelectrochemical sensing platform.

As a photoconductive semiconductor, bismuth sulfide ($Bi_2S_3$) has a direct band gap ($E_g$) of approximately 1.3 eV, which approaches the ideal value (1.34 eV) for maximum photovoltaic efficiency. The present approaches for preparing $Bi_2S_3$ overwhelmingly describe one-dimensional (1D) structures because of their highly anisotropic crystal structure that consists of infinite chains of covalently bound atoms. Gao *et al.* used several PILs as additives to modify the nucleation and growth of $Bi_2S_3$ materials with tailored sizes, dimensions, and architectures (nanowires, hexagonal plates, and mesoporous sheets); consequently, a tunable $E_g$ (from 1.54 to 1.95 eV) was observed owing to the quantum-size effect (Fig. 6a).[54] Intriguingly, the PIL-modified $Bi_2S_3$ nanowires can efficiently catalyze water oxidation, with an onset potential of OER occurring at approximately 1.46 V *versus* a reversible hydrogen electrode (RHE); however, the commercial counterpart is catalytically inert (Fig. 6b–d). It is proposed that the PIL chains grafted on $Bi_2S_3$ can modify its surface electronic structure, which leads to an oxidation state of Bi that has a high formal charge. Such merits further improve the catalytically active sites on $Bi_2S_3$ for optimum O-intermediate adsorption.

### 4.2 PIL–carbon composites

Carbon materials with excellent mechanical performance offer a number of advantages, namely, variable electron conductivity, good thermal conductivity, and chemical resistivity. In the past two decades, carbon materials, such as carbon nanotubes (CNTs), graphene, and fullerene, have attracted enormous attention ranging from material breakthroughs to diverse practical applications in electronics, optics, catalysis, and biology. However, most carbon nanomaterials without protection easily aggregate in solution, which limits their processing into high-performance devices. To achieve high loading and homogeneity

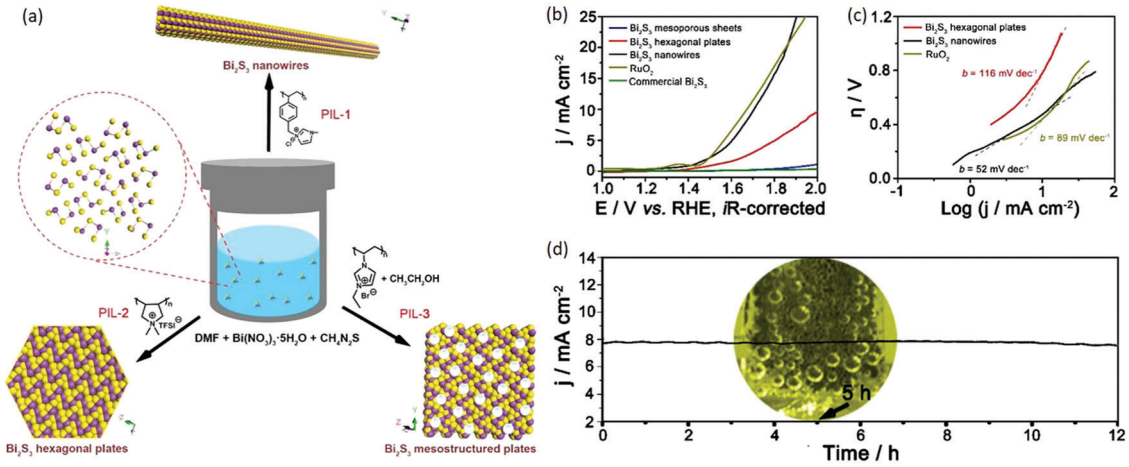


Fig. 6 (a) $Bi_2S_3$ crystals with morphological diversity prepared by using PILs as additives. (b) Polarization curves for OER on modified FTO electrodes comprising PIL-stabilized $Bi_2S_3$ crystals. (c) Tafel plots for various catalysts derived from (b). (d) Chronoamperometric response ($j$–$t$) recorded from the as-prepared $Bi_2S_3$ nanowires at a constant overpotential of 400 mV. Inset: Photograph showing $O_2$ bubbles accumulated on the $Bi_2S_3$-modified FTO electrode. Reprinted with permission from ref. 54. Copyright 2016 Wiley-VCH.

of carbon-based composites, defects in carbon (nano)materials are usually introduced by chemical functionality, sometimes resulting in an unfavorable deviation from their original properties. To integrate desirable properties of carbon materials without trading performance, PILs are employed as noncovalent dispersants for carbon materials in various solvents for producing devices by solution processing. In addition, the integration of PILs and carbon materials also creates new functions due to synergistic effects.

**4.2.1 PIL–CNT composites.** CNTs are widely used as electrochemical sensors, electrocatalysts or their support, lithium-ion battery cathodes and more due to their high surface area, excellent electron conductivity, and chemical stability. Research activities have employed CNTs as nanofillers to enhance the conductivity of electrodes. A highly conductive network requires extra effort to avoid the aggregation of CNTs in the composite matrix. PILs bearing imidazolium/pyridinium/triazolium moieties can directly attach to the surface of CNTs *via* π–π/π–cation interactions and readily disperse CNTs in solvents.

PIL–CNT composites have been extensively studied for energy storage and conversion. In 2009, Chen and coworkers reported a strategy to functionalize CNTs by *in situ* thermally initiated radical polymerization of an IL monomer, 1-ethyl-3-vinylimidazolium tetrafluoroborate, on a CNT surface.[104] CNTs covered by PILs can disperse in water and further serve as a medium to immobilize PtRu NPs (Fig. 7). Such PIL–CNT–PtRu composites electrooxidized methanol better than PtRu/CNTs without PILs as a surface modifier. This work points out that it is promising to use PILs as a "surface modifier" to incorporate with CNTs for enhanced performance. Alternatively, Heumann and coworkers used PIL-modified CNTs for scalable synthesis of single dispersed cobalt ions that were coordinated by PIL. The composites were tested as excellent catalysts for the oxygen evolution reaction (OER) because of the variations in the electronic structure of Co by coordinating with PIL, as well as the excellent conductivity contributed by CNTs.[105]

The synergistic effect between PIL and CNTs was clearly illustrated in a report by using redox-active catechol-bearing PIL–CNT composites as high-performance lithium-ion battery cathodes. The composite delivered a high reversible capacity of 247 mA h $g^{-1}$ at 0.2C with a capacity of 134 mA h $g^{-1}$ at 60C and retained 86% of its initial capacity during the prolonged 5000 cycling tests in comparison to a neutral polymer PAmcat in control experiments (Fig. 8). In comparison to the catechol units in the neutral polyacrylamide, the catechol moieties in the polyvinylimidazolium backbone bearing the $TFSI^-$ counteranion were anticipated to impart the following enhancements in Li-storage performance: (1) strong bonding between catechol PILs and CNTs *via* π–π/π–cation interactions, (2) superior cyclability without leaching of catechol groups into the organic electrolyte, (3) improved discharge potential due to electron-deficient imidazolium units in PILs, and (4) enhanced rate capability caused by favorable anion mobility at the electrolyte–electrode interface and in the bulk of the electrode.[106]

In addition to using PIL–CNTs for energy-related applications, such conducting composites can also be applied in electromechanical devices such as "smart" actuators. It has been revealed that enhanced conductivity and flexibility with high thermal stability and mechanical durability can be regulated by the weight content of CNTs in PIL–CNT composites.[107] The disclosed properties favor the potential application of PIL–CNT composites in electromechanical devices. Ricci and coworkers prepared dry electrochemical actuators using an imidazolium PIL and CNT composite gel as the electrode.[108] A direct correlation between the size of the anion ($Br^-$, $BF_4^-$, and $TFSI^-$) in the electrode and the resulting strain of the actuator could be detected, *i.e.*, large anions lead to high strain. Consequently, the displacement response of the actuator was proportional to the size of the counteranions. A maximum bending displacement of up to 0.5 mm was recorded under a low applied voltage of ±1 V. Alternatively, Lin *et al.* developed a porous PIL membrane composite with aligned CNTs in its matrix and

 

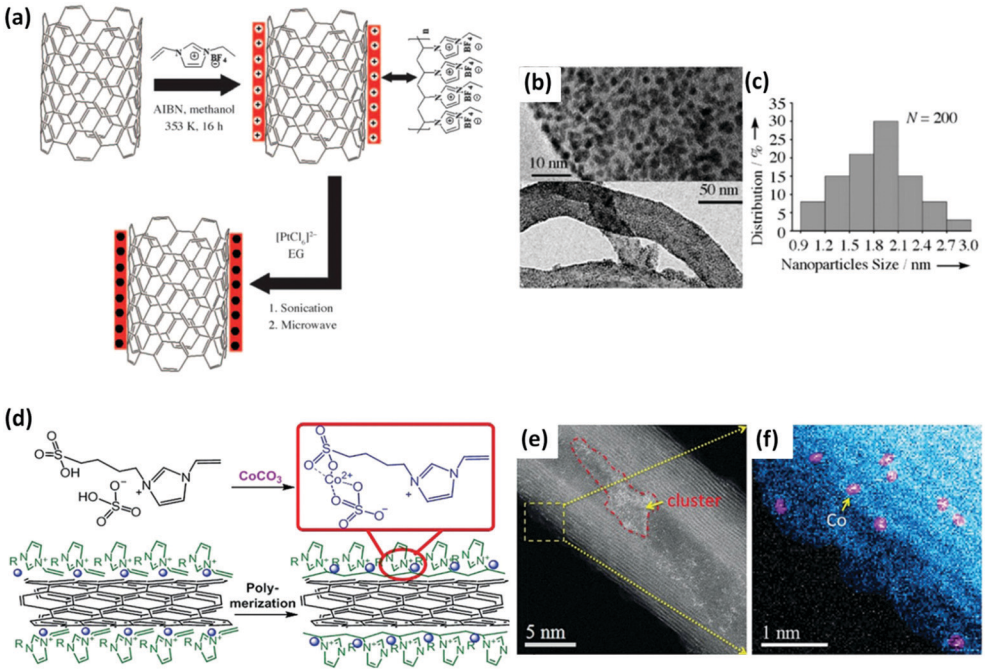


Fig. 7 (a) Synthetic scheme toward Pt/CNT–PIL nanohybrids. EG: ethylene glycol, AIBN: 2,2′-azobisisobutyronitrile. TEM images (b) and size distribution plot (c) of Pt NP/PIL nanohybrids. (d) Preparation scheme toward CoSSPIL/CNT. The blue spheres represent single Co species. The Scheme only shows the cation part on the CNT before and after polymerization. (e and f) HAADF-STEM images of CoSSPIL/CNT-1. Reprinted with permission from ref. 104 and 105. Copyright 2009 and 2018 Wiley-VCH.

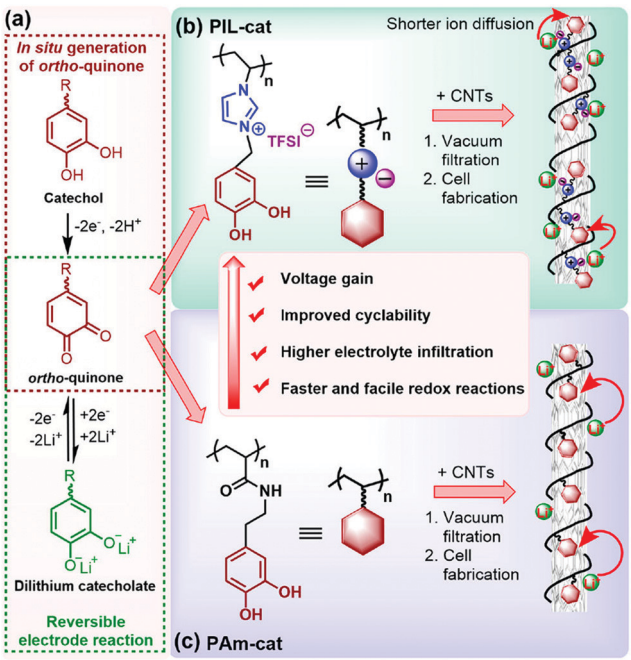


Fig. 8 Construction of catechol-based PIL/CNT buckypapers for LIBs. (a) *ortho*-Quinone/dilithium catecholate redox reaction. (b and c) Enhancement in the electrochemical performance of cationic PIL-cat (b) compared to its neutral counterpart PAm-cat (c). Reprinted with permission from ref. 106. Copyright 2018 American Chemical Society.

realized programmable, anisotropic actuation toward organic vapors. In this case, the actuating direction can be well predicted at a direction perpendicular to the longitudinal orientation of CNTs.[109]

**4.2.2 PIL–graphene composites.** Graphene and its derivatives as typical 2D materials attract global attention because of their extraordinary electronic, optical, thermal and mechanical properties. Due to the high specific area from the 2D structure at a single- or few-atom thickness, graphene is widely used as an ideal platform to improve the performance of the supporting materials for catalysts, electrodes, and sensors. However, the balance between the structural integrity and uniform dispersion of graphene is one of the issues to be solved. PILs as universal stabilizers are employed to wet the graphene surface *via* the well-known π–π/π–cation interactions, enhancing the compatibility of graphene with other materials. Texter and coworkers reported imidazolium PILs as stabilizers for graphene in water with weights up to 5%, surpassing previous "high concentration" results by two orders of magnitude. The delocalized π system of the imidazolium groups provided a simple mechanism to account for these backbone groups physically adsorbing to the $sp^2$ surfaces of graphene. Moreover, such graphene dispersions were rheo-optical fluids. Simple Couette shear fields were employed to align micron and submicron sheets over macroscopic areas, which is promising in future applications of a moderate shear coating (Fig. 9).[18]

The excellent dispersibility of the PIL–graphene composite allows for deposition on a broad range of substrates, including electrodes that can harness the electric properties of graphene for various sensing purposes. For example, Li and coworkers prepared a PIL–rGO composite as an electrochemical sensor for

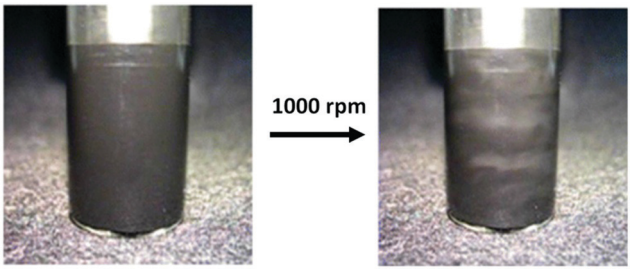


Fig. 9 Photograph of a vial containing PIL-stabilized graphene dispersion with an aluminum cylindrical stirrer (left) at rest and (right) at 1000 rpm. This change in reflectivity illustrates an anisotropic to a nematic transition. Reprinted with permission from ref. 18. Copyright 2014 American Chemical Society.

phenylethanolamine (PEA) determination at a high sensitivity. Comparing a PIL sensor and a bare electrode, the PIL–rGO sensor had the highest peak current response for PEA with a low detection limit of 0.002 μM due to the synergistic effect between rGO and PIL.[110] Similarly, such a PIL–GO composite system can also sense dopamine.[111]

PIL–graphene composites were explored as high-performance supercapacitors and were pioneered by Ruoff, Suh and coworkers.[51] These composites displayed a stable electrochemical response up to 3.5 V operating with a maximum energy density of 6.5 W h $kg^{-1}$ and a power density of 2.4 kW $kg^{-1}$. PILs coated on GO enhanced the compatibility of the composite with the IL electrolyte, *i.e.*, better wettability of the IL electrolyte on the composite materials, which synergistically increased the effective electrode surface area that was accessible to the electrolyte ions.

When graphene functions as a platform to offer a high specific surface area in the PIL–GO composite, the PILs can selectively collect the countercharged species, enabling selective isolation/separation of substrates. Nassernejad *et al.* developed a promising candidate for DNA delivery based on a PIL–3D GO framework. This PIL–GO composite has a strong electrostatic binding capability to a nucleic acid and a negatively charged cell membrane. Synergistically, the positively charged PIL–GO composite loaded with DNA of a small size was favorable for cellular uptake and intracellular trafficking, facilitating the use of the 3D composite as a suitable carrier for DNA delivery.[112] Alternatively, covering the $SiO_2$ surface with PIL–rGO composites can allow selective adsorption of acidic proteins such as ovalbumin due to the high specific surface area and the available electrostatic and π–π interactions.[82]

GO-Based mixed matrix membranes (MMMs) capable of anion exchange are scarcely explored in the literature. Szekely, Budd and coworkers prepared a series of PIL–GO nanocomposite anion exchange membranes (AEMs) with low GO loadings. The AEMs exhibited a high ion exchange capacity of 1.7–2.1 mmol $g^{-1}$, a good permselectivity of up to 0.99, and a relatively low area resistance that goes down to 2.9 U $cm^{-2}$. A trade-off between good selectivity and low resistance was investigated for membranes with low GO loadings (0.25–2.5%). The GO-based nanocomposite AEMs demonstrated excellent potential for electrodialysis with a permselectivity of 0.99 at a loading content of 1% GO.[113]

### 4.3 PIL–silica composites

Silica is cheap and chemically inert, and allows for irreversible surface modification through surface silanol groups. The functionalization of silica with a polymer can exhibit dramatic improvements in strength, modulus, heat resistance, gas permeability barrier properties and so on. One of the advantages of using PILs with diverse structures and functions to coat silica is to modify its surface characteristics, especially its hydrophilic/hydrophobic properties. It is well known that surface properties are important for the interactions between the material and the environment. In particular, wettability control has attracted extensive interest in the development of "smart" devices, *e.g.*, self-cleaning devices, discrete liquid droplet manipulators or tunable optical lenses. By immobilizing a poly[1-(2-acryloyloxyhexyl)-3-methylimidazolium bromide] brush layer onto the electrospun $SiO_2$ nanofiber surface *via* an SI-ATRP technique, an anion-directed molecular gating system was achieved. The use of a counteranion exchange reaction allowed the surface properties of the membrane to be reversibly altered between hydrophilic and hydrophobic; it enabled pores to withdraw or expel solvent molecules ($H_2O$), thus controlling the transport of probe molecules through the membrane (Fig. 10).[78] Similarly, the wettability of glass/silicon surfaces can be modulated by grafting different PILs.[114]

In addition to the surface modification of silica by PIL, silica serving as a nonconducting filler can increase the conductivity of both semicrystalline and amorphous polymer electrolytes, which provides the possibility of generating complementary functionality (*i.e.*, structural stability) and transport tunability for ion-conducting materials. For example, Ye and coworkers reported a PIL-functionalized mesoporous silica nanoplate, which increased the ionic conductivity of the PIL/IL electrolyte by 1130% at ~30 °C because of a significant decrease in the ion transport activation barrier (approximately 10 kJ $mol^{-1}$).

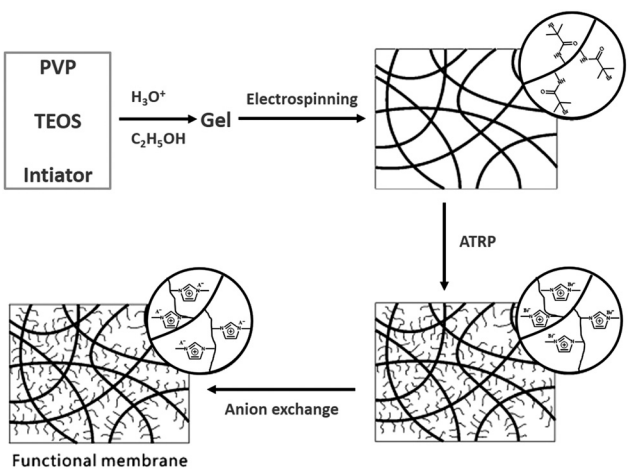


Fig. 10 Schematic illustration of the preparation of the PIL brush-coated electrospun silica–PIL composite membrane. Reprinted with permission from ref. 78. Copyright 2010 Royal Society of Chemistry.

Such nanofillers simultaneously conferred both a high ionic conductivity of $\sim 10^{-3}$ S cm$^{-1}$ at 130 °C with only 15 wt% IL loading and excellent IL immersion and retention properties to the mixed PIL/IL polymer electrolytes. The nature of the disposition and the ionic channel junctions, formed through nanoscopic modification, is expected to facilitate ion transfer through the ionic channels.[115] It can also be extended to other PIL–silica composites such as pyrrolidinium-based PIL–silica hybrid ionogel electrolytes (HIGEs)[116] or core–shell $SiO_2$–poly-[*p*-vinylbenzyl-trimethylammonium tetrafluoroborate] ($SiO_2$–P[VBTMA][$BF_4$]) composites with tunable structures as high-performance ion-conducting systems.[117]

The combination of nanoporous silica with PIL can serve as a functional porous material for various adsorption and separation events, including $CO_2$ capture, antidiabetic drug extraction, ion exchange, and reversed-phase and liquid chromatography. The presence of ions on PILs enhances $CO_2$ absorption capabilities, which can be further improved by a nanoporous silica component in the composite. For example, P[VBTMA][$BF_4$]-functionalized mesoporous silica (meso-silica) hybrids can rapidly adsorb $CO_2$ at a capacity of 0.4 mmol g$^{-1}$ at 30 °C from a simulated flue gas containing 10 vol% $CO_2$.[118] Similarly, polymerizing 1-(2-acryloyloxyundecyl)-3-methylimidazolium bromide ([mC11C1Im]Br) that is already attached onto a mercaptopropyl-functionalized silica Sil-MPS results in a hybrid Sil-pC11C1Im. The carbonyl, polar imidazolium, and hydrophobic alkyl chain groups in the composite as interaction sites show a considerably high molecular-planarity selectivity toward polycyclic aromatic hydrocarbon isomers, additional anion-exchange capability and available hydrophilic interaction.[119] Moreover, silica-coated iron oxide NPs modified with an imidazolium PIL ($Fe_3O_4$@$SiO_2$@PIL) were used as a sorbent for magnetic solid-phase extraction (MSPE) and determination of trace amounts of antidiabetic drugs in human plasma. The modification of PILs combined the magnetic response of NPs with IL characteristics and improved the stability, reusability, mass transfer capacity and diffusion routes of the nanoscale sorbent.[120]

### 4.4 PIL–metal salt composites

Metal salts can easily complex with PILs *via* electrostatic/coordination interactions. To date, the most extensively investigated PIL–metal salt composites are the main group of metal–PIL systems, such as $Li^+$/$Na^+$–PIL. When applied in Li-ion batteries as solid electrolytes, PILs are usually combined with IL-based electrolytes (a solution of Li/Na salts in ILs) to enhance their inherently limited ion conductivity. The chemical affinity between PILs and ILs prevents them from phase separation; additionally, in comparison with traditional solid electrolytes, the resulting composite electrolytes are provided with outstanding integrated performances, including a high ion conductivity, a wide electrochemical window, a favorable plating morphology of the Li metal, and a device that does not leak and is noncombustible at room temperature.[68] Zhou *et al.* fabricated a hierarchical PIL-based solid electrolyte (HPILSE) by integrating a PDADMADTFSI porous membrane and a polymerized 1,4-bis-[3-(2-acryloyloxyethyl)imidazolium-1-yl]butane TFSI (C1-4TFSI) cross-linking network within an IL 1-ethyl-3-methylimidazolium TFSI (EMITFSI)-based electrolyte, where the cross-linked C1-4TFSI maintained the entire mixture in a quasi-solid-state to avoid liquid leakage even at high temperature. The as-prepared PDADMADTFSI porous membrane and a suitable amount of the EMITFSI-based electrolyte provided a tensile strength of 2.4 MPa and an ion conductivity above $10^{-3}$ S cm$^{-1}$ at 25 °C. Because of the robust interfacial contact between the HPILSE and electrodes going against the electrode volumetric changes during charge/discharge cycles, when this system is applied in Li-ion and Na-ion batteries, better electrochemical performances can be achieved for the assembled $LiFePO_4$/HPILSE/Li and $Na_{0.9}[Cu_{0.22}Fe_{0.30}Mn_{0.48}]O_2$/HPILSE/Na polymer cells (Fig. 11).[73]

In addition to being employed as solid-state electrolytes, PIL-immobilized metal salts containing both metal centers (Lewis acids) and ionic units (nucleophiles) can serve as bifunctional catalysts in heterogeneous reactions. The combination of nanobelt α-$CuV_2O_6$ with a porous PIL derived from a cross-linked solid acid P(EVPI-Br) (Fig. 12) generated a binary catalyst and afforded a 63.1% yield in the one-pot one-step conversion of fructose into 2,5-diformylfuran ($O_2$, 135 °C, 3.5 h). The hydrophilic surface of P(EVPI-Br) enabled the preferential adsorption of fructose on the acid sites; in contrast, α-$CuV_2O_6$ strongly adsorbed 5-hydroxymethyl furfural (HMF) but had weak affinity to fructose (Fig. 12). Such surface wettability-controlled adsorption features inhibited the oxidation of fructose and facilitated the transfer of HMF to the oxidative sites on α-$CuV_2O_6$, and thus, its timely conversion into the final product.[121] Similarly, the PIL–metal salt hybrid provides an ideal platform to produce diverse binary catalysts for task-specific catalysis.[75] For example, introducing $CrCl_3 \cdot 6H_2O$ into $SO_3H$-functionalized poly(1-vinyl-3-propanesulfonylimidazolium) (PVMPS) with $PW_{12}O_{40}$ and Cl as counteranions provides bifunctional catalysts carrying Brønsted/Lewis acidic groups, which effectively convert biomass including fructose, glucose, and cellulose into HMF in the presence of DMSO-mediated solvents.[61]

The incorporation of metal ions into PIL-containing membranes can also influence the gas separation process. The metals sometimes can serve as carriers for enhanced affinity to certain gases; for example, a high ethylene absorption capacity can be achieved by a mixture of PILs containing the [TFSI] anion and the AgTFSI salt.[70] Bara and coworkers recently explored PIL–IL membranes containing the $[CuCl_2]^-$ anion as a gas separator, in which enhancement of both gas permeability and ideal gas pair selectivity was observed for $CO_2/N_2$ and $H_2/N_2$ separation in the composite membranes with respect to the neat poly([$C_4$VIm][TFSI]). The $[CuCl_2]^-$ anion was able to selectively and reversibly bind $CO_2$ molecules to increase the solubility of $CO_2$ in the composite.[122]

In addition to the aforementioned applications, PILs can synergistically work with functional metal sites to develop "smart" hybrids or devices.[123–129] By incorporating a redox-active metal site into a polyferrocenylsilane derivative (PFS–$SO_3$), Vancso and coworkers developed organometallic PFS–PIL

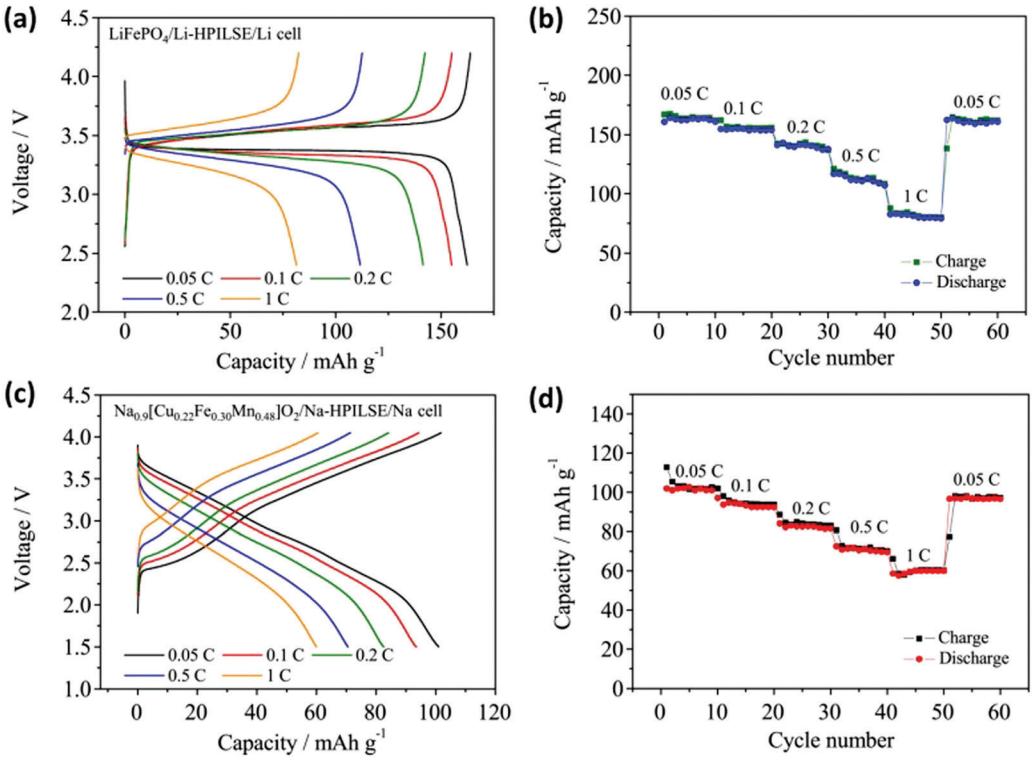


Fig. 11 Electrochemical characterization of Li-ion batteries exploiting HPILSE. (a) Typical charge and discharge curves and (b) rate performance of the $LiFePO_4$/Li-HPILSE/Li cell. Electrochemical characterization of Na-ion batteries exploiting HPILSE. (c) Typical charge and discharge curves and (d) rate performance of the $Na_{0.9}[Cu_{0.22}Fe_{0.30}Mn_{0.48}]O_2$/NaHPILSE/Na cell. Reprinted with permission from ref. 73. Copyright 2017 Elsevier.

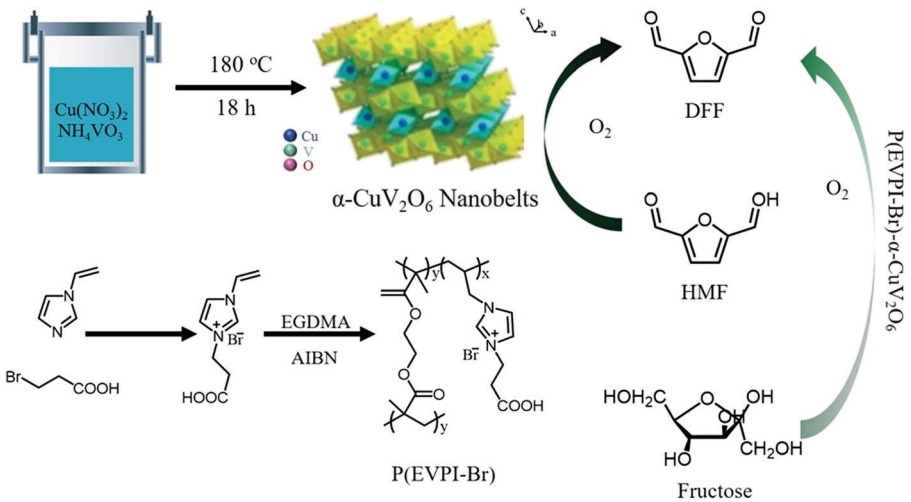


Fig. 12 Synthesis of $\alpha$-$CuV_2O_6$ and MPIL P(EVPI-Br) for the conversion of 5-hydroxymethyl furfural (HMF) and fructose into DFF. Reprinted with permission from ref. 121. Copyright 2017 Royal Society of Chemistry.

hybrids for electrochemical sensing (Fig. 13), switchable porous materials, plasmonic NPs and smart windows due to their redox- or electrical-responsive behaviors.[126] Moreover, by introducing β-CD into this PIL–ferrocene composite system, a ''smart'' velcro-mediated polymer could be achieved by responses to redox stimuli. The synergistic effect between the PIL and PFS created a family of ''smart'' composites for broad areas.[128,129]

### 4.5 PIL–polyoxometalate composites

POMs, anionic metal oxide clusters with several to tens of negative charges, have been extensively investigated in catalytic applications due to their unique electrical and optical properties. However, their intrinsic hydrophilicity causes difficulties in their separation and recycling during catalysis. A number of strategies have been developed for the heterogenization of POM catalysts, including phase transformation, microemulsion formation,

 

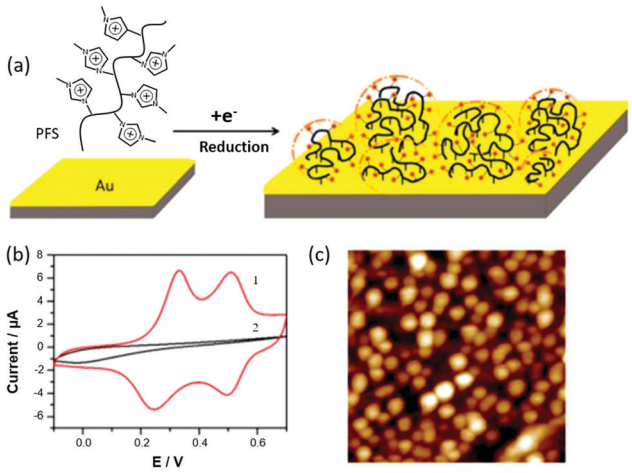


Fig. 13 (a) Schematic illustration of the electrografting of PFS-MID-Cl in ILs. (b) Cyclic voltammogram of a PFS-modified Au electrode (1) with a deposition potential of −2.2 V and (2) with a deposition potential of −0.8 V in 0.1 M $NaClO_4$; this was conducted using an Ag/AgCl reference electrode and a Pt counter electrode at a scan rate of 50 mV $s^{-1}$. (c) AFM height image of PFS grafts on Au using a tapping mode in air; scan size: 1 μm × 1 μm, z-scale: 30 nm. Reprinted with permission from ref. 126. Copyright 2014 American Chemical Society.

encapsulation by inorganic or organic cations, and immobilization into a polymer or a silica matrix. Assembly of POMs with polycations is revealed to be a successful example for preparing heterogeneous POM catalysts, which is beneficial for adjusting the solubility, redox properties, and surface microenvironment of POMs. To date, PILs have been used to pair with heteropolyanions to prepare diversified PIL–POM hybrid catalysts in various reactions, including oxidation of sulfides to sulfoxides, hydroxylation of benzene, photodegradation, epoxidation and oxidation of 5-hydroxymethylfurfural. Doherty *et al.* immobilized $[PO_4\{WO(O_2)_2\}_4]^{3-}$ on a pyrrolidinium-functionalized PIL to produce a $[PO_4\{WO(O)_2\}_4]$@PIL composite, which exhibited high efficiency and long-term activity for the oxidation of allylic alcohols and alkenes compared with PIL-free $[PO_4\{WO(O)_2\}_4]$@silica composites. These comparisons underpin the potential benefits of preparing a PIL support for robust POM catalysts in reactions.[130]

Wang and coworkers systematically investigated PIL–POM composites in heterogeneous catalysis. They developed hierarchically nanoporous PILs as supports for immobilizing POMs. In catalytic reactions, the mesoporosity with a relatively high specific surface area benefits the loading and good dispersion of the active POM species as well as the accessibility of substrates to active sites, while the availability of both meso- and macropores favors the improvement of mass transport. For example, a hierarchical meso-macroporous PIL (HMP) was synthesized by radical polymerization of a 1-allyl-3-vinylimidazolium chloride [AVIm]Cl monomer using a tri-block copolymer P123 poly(ethylene oxide)-*block*-poly(propylene oxide)-*block*-poly-(ethylene oxide) (PEO–PPO–PEO) as a soft template; this process was followed by the removal of P123, and thus, a highly dispersed Keggin-structured phosphotungstic anion $PW_{12}O_{40}^{3-}$ (PW) was immobilized inside the mesopores through anion exchange (Fig. 14a). This composite acted as a heterogeneous catalyst in the liquid-phase epoxidation of *cis*-cyclooctene with $H_2O_2$, showing superior catalytic activity compared with that of the phosphotungstic acid $H_3PW$ and hybrid catalyst [AVIm]–PW (Fig. 14b).[131]

Similar hierarchically nanoporous PIL–POM systems have been explored, *e.g.*, poly(divinylbenzene-3-*n*-butyl-1-vinylimidazolium) (P-$[DVB\text{-}VBIM]^+$)-containing a Keggin HPA-anion ($PMo_{10}V_2O_{40}$) or mesoporous ionic network-POM composites. These catalysts are highly active toward hydroxylation of benzene with $H_2O_2$[132] and ambient selective aerobic oxidation

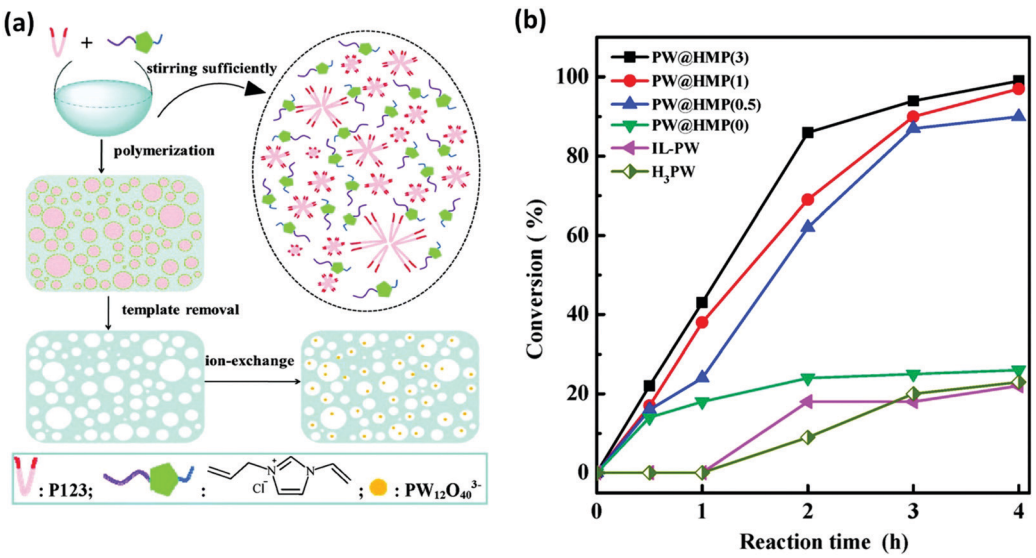


Fig. 14 (a) Synthetic process of hierarchical meso-macroporous PILs by using the soft template P123. (b) Conversion of *cis*-cyclooctene as a function of reaction time for PW@HMP(*x*)-catalyzed liquid-phase epoxidation with $H_2O_2$. Reaction conditions: *cis*-cyclooctene (5 mmol), $H_2O_2$ (4 mmol, 30 wt%), methanol (1 mL, as the solvent), 60 °C, 4 h. Reprinted with permission from ref. 131. Copyright 2015 Royal Society of Chemistry.

of HMF into 2,5-diformylfuran with $O_2$, outperforming the PIL-free POM catalysts.[133]

In addition to using nanoporous PILs as an advanced support for immobilizing POM catalysts, the surface modifications of POM catalytic sites are another aspect to enhance catalytic performance. In particular, the development of amphiphilic POM composites is important in heterogeneous catalysis, especially in aqueous/oil biphasic systems, to balance activity and selectivity. By harnessing the unique properties of PILs with tunable cations and/or anions, it is feasible to improve the adaptability of POMs toward the external environment for task-specific applications. Leng *et al.* designed a PIL copolymer containing units of dodecyl imidazolium IL (DIM) and carboxylic acid-functionalized imidazolium IL (CIM) to fabricate an amphiphilic POM–PIL composite through ion exchange with the $[PO_4(WO_3)_4]^{3-}$ species. The hydrophobic alkyl chains ($-C_{12}H_{25}$) and hydrophilic carboxyl acid groups (–COOH) were introduced to supply a unique interfacial amphiphilic microenvironment for $H_2O_2$-based epoxidation of alkenes. In this case, the peroxo-tungstate species in POM anions acted as the active centers for epoxidation reactions, whereas the amphiphilic catalyst structure served as a "trapping agent" for both the hydrophobic alkene substrates and the hydrophilic $H_2O_2$ molecules. Therefore, the mass transfer in the liquid–liquid–solid media was accelerated, and the catalytic activity was promoted.[134] The combination of porous PIL supports featuring an amphiphilic surface is effective for immobilizing POM catalysts. Recently, a polyhedral oligomeric silsesquioxane (POSS)-derived mesoporous composite (by copolymerization of dicationic imidazolium IL [1,1-(butane-1,4-diyl)-bis(3-vinylimidazolium)]$Br_2$ (BM) with octa(*N*-vinylimidazole silsesquioxane) POSS) has been employed to combine with a Keggin-type POM, yielding amphiphilic mesostructured POM-based ionic hybrid catalysts. The mesoporous structure and the amphiphilic catalyst surface, which allow for rapid diffusion of the reactants into the reactive POM centers, are responsible for the excellent catalytic performances in the epoxidation reaction with $H_2O_2$.[135]

### 4.6 PIL–organic polymer composites

Organic polymers possess some unique attributes, including ease of production, light weight, and tunable thermal and chemical stability, which are desirable to integrate them with other functional materials for composites. PILs as functional polyelectrolytes can be combined with polymers for enhanced mechanical strength while simultaneously maintaining ionic conductivity.[136] Moreover, due to the high compatibility between PILs and a broad range of polymer substances, PILs can be used to polymerize on polymer particle seeds to grow PIL–polymer composite particles. These composite particles have the advantage of low cost and easy processability in comparison to PIL homopolymer particles. In the case of the core–shell composite particle consisting of a core from a commercial polymer and a PIL shell, the films and pellets prepared from the composite particles are also promising for the design of ionic conductive materials, in which the ionic conductive PIL shell forms effective ion transport paths. Recently, such composite particles have been achieved in PIL–PMMA (poly(methyl methacrylate)) composite particles with either a sea-island structure consisting of PIL domains or core–shell PIL–PMMA structures (Fig. 15a). These results are consistent with the theoretical considerations that are based on the spreading coefficients calculated from the interfacial tensions. Moreover, hydrophobic PILs of high polarity are effective for controlling the morphologies of the final composite particles.[137]

In addition to the morphology control of PIL–polymer composites, a synergistic effect can be engineered by placing a polymer, bearing responsive properties, within PIL composite particles for enhanced properties. For instance, a monodispersed PIL microsphere coated with a semiconducting polyaniline (PANI) shell shows an enhanced electroresponsive electrorheological effect with a lower power consumption in comparison to neat PIL microspheres (Fig. 15b).[138] The authors claimed that the semiconducting PANI shell could effectively limit the irreversible ion leakage of PIL microspheres and improve the particle polarizability, resulting in decreased power consumption and an enhanced electroresponsive electrorheological effect. Alternatively, when using inherently conducting PANI as a core, they developed a type of PIL-encapsulated PANI composite particle that overcame the surface charge character of pure PIL particles and enhanced the electrorheological effect.

PILs can also directly complex with another polymer to form porous NPs. We recently reported ionic complexation between the poly(3-cyanomethyl-1-vinylimidazolium) series (PCMVImX, X = $TFSI^-$, $PF_6^-$, $BF_4^-$, or $Br^-$ anions) and PAA that yielded insoluble aggregated nanoparticles.[139] The powders of these particles possessed micro- and mesopores with an $S_{BET}$ and a pore volume of up to 310 $m^2\ g^{-1}$ and 0.98 $cm^3\ g^{-1}$, respectively. They were stable when refluxed in ethanol as well as several other organic solvents (80 °C) for 24 h. This composite was further loaded with a copper salt and served as a heterogeneous catalyst for the aerobic selective oxidation of C–H bonds.

In addition to the synthesis of composite NPs, the most obvious advantage of combining PILs with other polymers is membrane fabrication. In this process, since the PIL is an ionic polymer, the compatibility, especially the charge compensation, between the PIL and the other polymers should be carefully considered to produce a uniform composite structure that is beneficial for material performance. For example, the above-mentioned PIL–PAA complex can be extended to fabricate hierarchically structured nanoporous ionic complexation membranes. The pore character can be tuned by controlling the charge density, the molecular weight of the acids, and the additives. Such membranes have either a homogeneous porous cross-section or a gradient distribution of pore sizes.[64] In addition to ionic complexation driven by electrostatic interactions, other supramolecular interactions can also be considered as a tool for composite film fabrication. An example is illustrated here by the combination of poly(vinylidene fluoride) (PVDF) with a poly(2-(dimethylamino)ethyl methacrylate) methyl chloride; in this case a film is fabricated through noncovalent interactions between the localized cationic ions of the PIL and the polar $-CF_2$ group of PVDF, which results in

 

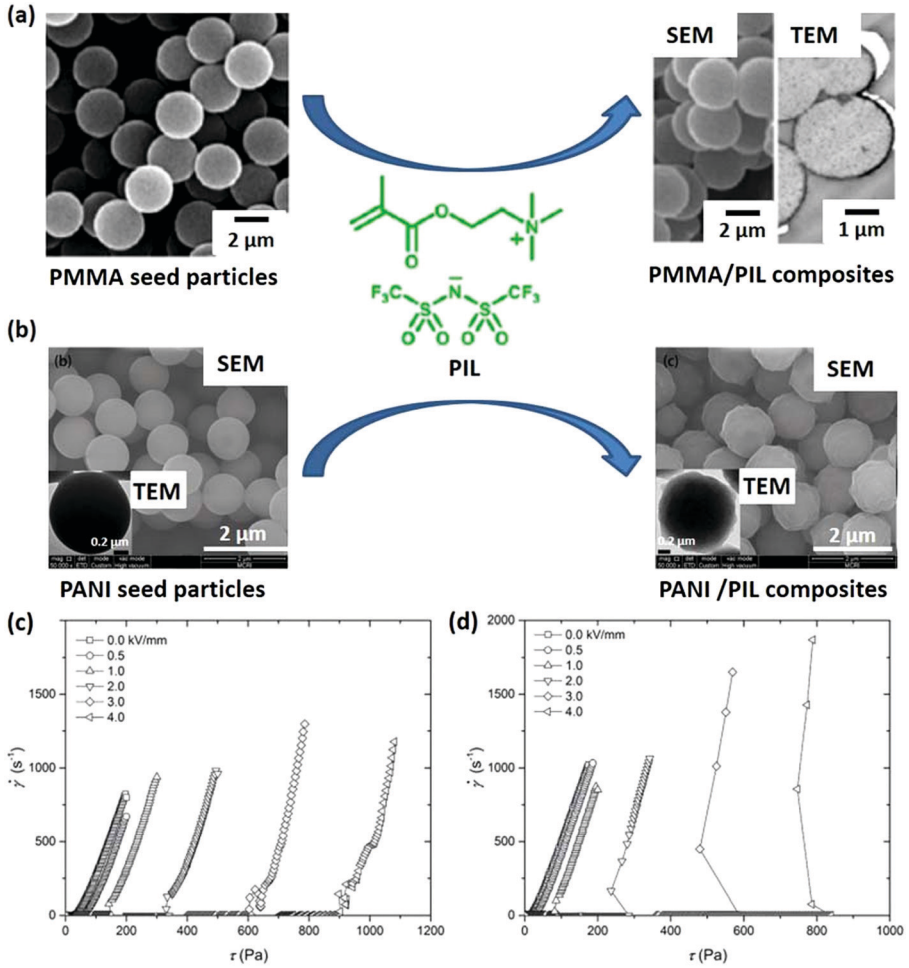


Fig. 15 (a) PMMA (left) and PMMA/PIL (right) composite particles. (b) PANI (left) and PANI/PIL (right) composite particles. (c) Flow curves of shear rate *versus* shear stress for the electrorheological suspensions of PIL microspheres. (d) PANI/PIL microspheres. Reprinted with permission from ref. 137 and 138. Copyright 2013 American Chemical Society and Copyright 2018 Wiley-VCH.

a PIL–PVDF composite film featuring excellent ferroelectric properties.[140]

PIL–polymer membranes are useful in electrochemical devices. In particular, PIL-based electrolytes are selected for memory devices because of their advantages of mechanical stability, safety, good processability and moderate ionic conductivity. Li *et al.* constructed a three-terminal nonvolatile memory device by combining a poly[1-(4-vinylbenzyl)-3-butylimidazolium tetrafluoroborate] (PVBIT) PIL layer, a hydrophilic polythiophene and a poly(3-carboxypentylthiophene) (P3CPT) active layer. Memory effects could be obtained at high write/erase voltages (+3/3 V) and a low read voltage (0.5 V) in the three-terminal device. Simultaneous monitoring of both the "write" and "read" operations revealed an instantaneous response and a fast switching speed (Fig. 16). The memory behavior of the composite could be attributed to the synergistic effect between the polarization of the polythiophene backbone due to the P3CPT polaron and then stabilization through both the carboxylate anions and the $BF_4$ anions that immigrate from the polyelectrolyte layer.[141]

The use of ILs in polymeric membranes is known to elevate the electrochemical performance of proton exchange

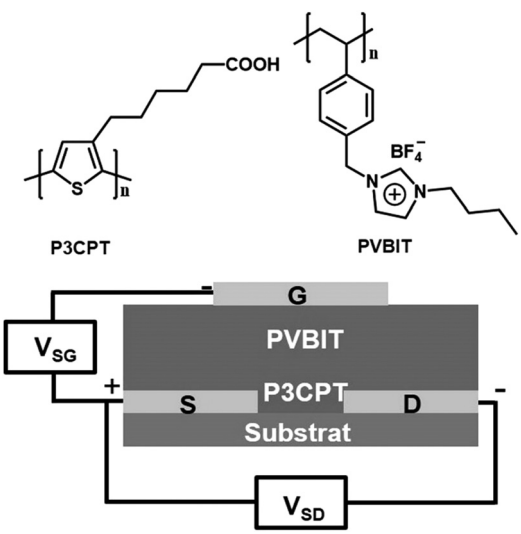


Fig. 16 Chemical structures of the materials used in a nonvolatile memory device. Reprinted with permission from ref. 141. Copyright 2015 Wiley-VCH.

membrane-based fuel cells (PEMFCs). However, they suffer from drawbacks such as IL drain and a decrease in mechanical properties. The incorporation of PILs is anticipated to provide a continuous pathway for the IL character (which is present in the repeating unit of the polymer), while eliminating the issue of IL drain. PILs also retain the unique properties of ILs to a certain extent (*e.g.*, ionic conductivity, thermal stability, tunable solution properties and chemical stability), which in combination with their intrinsic polymer properties are expected to offer better benefits than simple ILs. Kharul and coworkers reported a membrane composed of homogeneously mixed PDADMA–trifluoromethanesulfonate (P[DADMA][TFMS]) and polybenzimidazole (PBI-I) for PEMFCs with a proton conductivity of up to 0.07 S $cm^{-1}$ at 150 °C. Single-cell evaluations of the membrane have been successfully demonstrated using $H_2/O_2$ at 160 °C under nonhumid conditions with an excellent current density of 1632 mA $cm^{-2}$. The good miscibility of the components in the membrane worked synergistically to enhance the physical and electrochemical properties.[142]

The PIL–polymer hybrid membranes can also be used in separation and absorption. Yan and coworkers prepared wastewater treatment media consisting of PIL-grafted polypropylene (PP) nonwoven fabrics by surface-grafting polymerization of IL monomers and photochemical crosslinking. The as-prepared PIL–PP fabrics exhibited excellent switchable oil/water separation (>99%) and dye adsorption performance (410 mg $g^{-1}$).[143] Another type of PIL–polymer composite membrane with sulfonate ionic cross-links and free sulfate groups exhibits both high flux and water selectivity in dehydrating various alcohols due to its strong interpolyelectrolyte binding, higher hydration capability and sorption separation factor.[144]

### 4.7 PIL–organic molecule composites

Organic molecules with highly designable structures and abundant electronic, electrical, magnetic, optical, biological, and chemical properties are extensively explored in materials science. The combination of PILs with organic molecules containing an abundance of functional sites may modulate the physical properties of PILs and generate new functional composite materials. One of the major families of PIL–organic molecule composites is a host–guest complex, which employs well-established noncovalent interactions to achieve stimulus-responsive functional materials. For example, Ritter and coworkers reported the pseudo-lower critical solution temperature (LCST) effect of poly(1-vinyl-3-butylimidazolium TFSI) (poly[vbim][TFSI]) based on the solubility change of poly([BVIm][TFSI]) due to supramolecular complexation effects. It was shown that β-CD formed stable complexes with $TFSI^-$ at room temperature. At high temperatures, β-CD slipped off from the anion, and the resulting noncomplexed polymer precipitated (Fig. 17). This pseudo-LCST effect of PIL may provide new applications for temperature-sensitive gels.[66] Similarly, Yan and coworkers reported shape memory PIL gels with controllable macroscopic swelling *via* noncovalent host–guest interactions between β-CD and TFSI anions. The quick swelling and shape memory behavior of these PIL gels were observed in a β-CD aqueous solution due to a hydrophobic-to-hydrophilic transition induced by the β-CD/TFSI inclusion complexes; additionally, the PIL gel underwent only slight swelling in the presence of water.[145]

PILs can also complex with organic acids (aromatic and aliphatic carboxylate acids with carboxylate groups ≥2) based on electrostatic interactions. The high ionic cross-linking density of the system solidifies and stabilizes the ionic network with minimum chain mobility. The generated nanoporous rigid solids show $S_{BET}$ values ranging from 230 to 350 $m^2$ $g^{-1}$ with tunable pore volumes from 0.63 to 1.54 $cm^3$ $g^{-1}$. The porous complex composites are more effective in removing methyl orange (MO) dye from an ethanol solution than an activated carbon and mesoporous silica with similar or even higher $S_{BET}$ values; this effect is suggested to stem from the synergistic combination of the polarity, mesopores, ionic character as well as the fine dispersibility of the composite particles in ethanol.[63,146] Alternatively, such ionic porous complex composites can form on the surface of $Fe_3O_4$, which serves as a magnetic solid phase extraction (MSPE) adsorbent with enhanced adsorption capacity due to the synergistic effect stemming from multiple contributions by the components in the composites, *i.e.*, inclusion, hydrophobicity, π-complexation, and porosity.[147]

In addition to applications in adsorption, a PIL–organic molecule composite can potentially be used as a sensor. Very recently, we have developed a triazolium PIL–TA (trimesic acid) ionic complex membrane bearing two concurrent structure gradients; the two gradients include an electrostatic complexation (EC) degree gradient and a density distribution gradient for a carbene–$NH_3$ adduct (CNA) along the membrane cross-section (Fig. 18). The two gradients could independently exert a response to organic solvents/compounds and weak acids. In particular, it expressed the highest sensitivity among all soft proton actuators toward acetic acid at the $10^{-6}$ mol $L^{-1}$ M level in aqueous media. It was also capable of discriminating between weak acid species with p$K_a$ values of 3–5 by actuation. Moreover, through the competing actuation of the two gradients, it was able to monitor an entire process of chemical reactions that combined multiple steps and carried multiple stimuli with competitive interactions.[148]

### 4.8 PIL–MOF/POF composites

Metal–organic frameworks (MOFs) and porous organic polymers (POFs) have emerged as a new class of anoporous materials and have been extensively explored in applications including gas storage, separation, catalysis, and sensing. Much effort has been devoted to developing hybridization of MOFs/POFs and polymers with improved functions.[149] The polymer hybrid with MOFs/POFs can be achieved either by encapsulation or by surface modification, both of which may lead to intriguing properties. PILs are ionic in nature with highly tunable scaffold structures and these scaffolds are popular for combining with MOFs/POFs to form new composites.

Currently, PIL–MOF/POF composites have been explored for catalytic applications, particularly for $CO_2$ cycloaddition reactions. In this case, the counteranions in PILs serve as

 

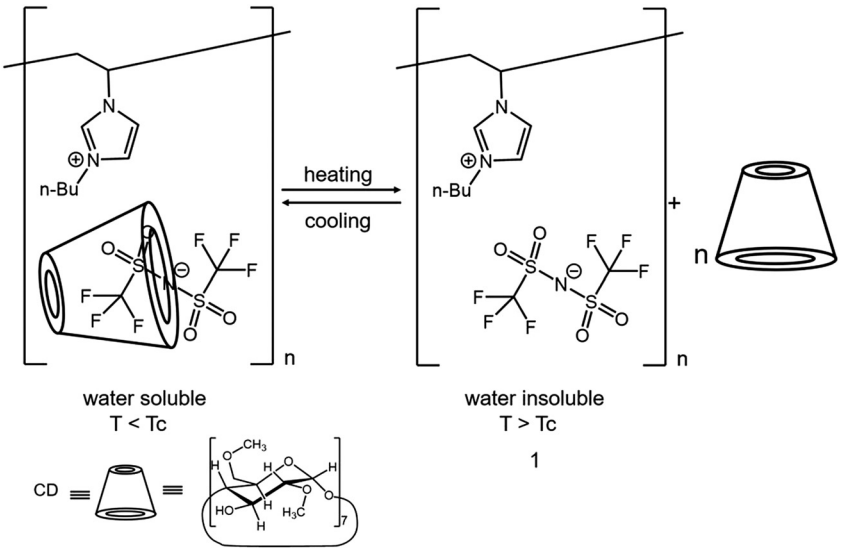


Fig. 17 Pseudo-LCST behavior of the poly[vbim][TFSI]–CD composite. Reprinted with permission from ref. 66. Copyright 2008 American Chemical Society.

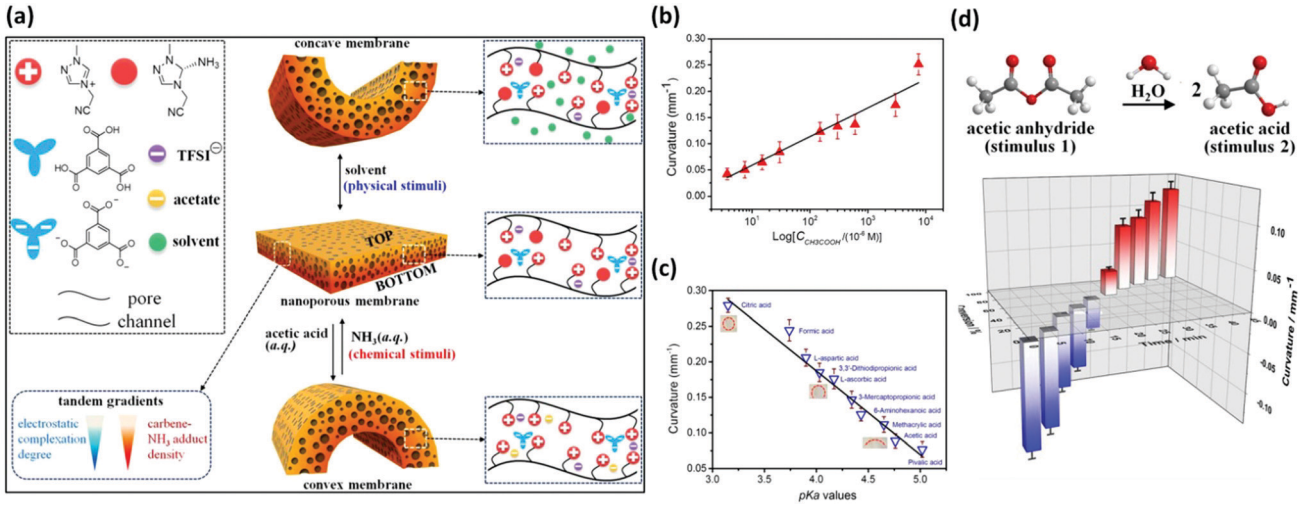


Fig. 18 (a) Schematic illustration of the bending mechanism derived from the tandem gradients of the membrane actuator by external stimuli. (b) Linear correlation of the membrane curvature against $CH_3COOH$ concentration. (c) Detection of a broad range of weak acids with different p$K_a$ values by a Ptriaz-TA membrane actuator (1 mm × 25 mm × 80 μm). Insets: Photographs of the membrane stripe in different acid solutions. (d) The cascade actuation of the tandem-gradient Ptriaz-TA membrane (1 mm × 25 mm × 120 μm) for monitoring a chemical reaction. (up) Ball-stick models representing the two stimuli driving the cascade actuation. (down) 3D histogram by plotting the conversion of acetic anhydride against the corresponding curvature of the membrane stripe. Reprinted with permission from ref. 148. Copyright 2018 Nature Publishing Group.

nucleophilic agents, while the metals in MOF/POF serve as Lewis acid sites that cooperate to catalyze the reaction. For instance, the combination of a porous zinc–porphyrin framework (P-POF-Zn) and PIL can catalyze the cycloaddition reaction of $CO_2$ and propylene oxide, demonstrating a TOF of 433 $h^{-1}$.[150]

In view of the flexible nature of linear polymers, their functional moieties have significant movability, thereby exhibiting properties similar to those of their homogeneous counterparts, which makes them promising candidates to be utilized instead of molecular catalysts. The advantage of a nanoporous POF or MOF enables the encapsulated linear PIL to maintain its flexibility; meanwhile, the flexible and mobile catalytic moieties on the linear polymer cooperate with the active sites anchored on the COF pore walls, which is promising for synergistic catalysis. Ma and coworkers deposited linear PILs in close proximity to Lewis acid active sites (Cu) anchored on the wall surfaces of a COF. In addition to the synergistic effect of catalytic sites in the composite, the essential catalytic components enriched in the confined space were beneficial for boosting cooperation and promoting catalytic efficiency toward cycloaddition reactions with atmospheric $CO_2$. This work also afforded an amenable route to

bridge natural and artificial systems.[151] Similarly, synergy between PILs and porous hosts to enhance $CO_2$ capture and conversion has been observed in Zn–$PPh_3$ integrated porous organic polymers[152] or PIL–MIL-101(Cr) composites.[153]

Such porous hybrids functionalized with ionic species are also useful in selective adsorption and separation. An example was a hierarchically porous structure produced by Guan, Wang and coworkers; they combined a hydrophobic mesoporous PIL copolymer (by copolymerization of amine-functionalized imidazolium-IL monomer and divinylbenzene) with a subsequent modification of ZIF-8 on the surface of a PIL *via* a facile *in situ* growth procedure. ZIF-8@PIL showed excellent $CO_2$ adsorption (0.80 mmol $g^{-1}$ at 298 K) and diffusion ($1.50 \times 10^{-3}$ $s^{-1}$) properties in comparison to the pure PIL (adsorption capacity: 0.51 mmol $g^{-1}$ at 298 K, diffusion rate: $1.11 \times 10^{-3}$ $s^{-1}$). In particular, small micropores were generated in the growth process due to strong coordination interactions between the amino-alkyl chain on the surfaces of the PIL and ZIF-8, which was beneficial for $CO_2$ storage at low pressure.[154] In addition, ZIF-8 nanoparticles and PILs were mixed for the preparation of MMMs for natural gas sweetening and postcombustion $CO_2$ capture.[155] Improved gas permeability without much scarifying $CO_2/N_2$ and $CO_2/CH_4$ selectivity was achieved as compared to their PIL counterparts. Nabais *et al.* used different MOFs (MIL-53(Al), $Cu_3(BTC)_2$ and ZIF-8) as fillers for PIL–MOF MMMs, aiming to maximize the membrane performance toward the purification of syngas. The membrane permeability was considerably influenced by the intrinsic characteristics of the incorporated MOFs, namely, their porous volume, cavity topology and surface area. Among the three different types of MMMs, membranes based on MIL-53(Al) showed the highest improvement in ideal selectivity (up to 13.3), while membranes based on ZIF-8 achieved the highest results for $CO_2$ permeability, up to 97.2 barrer with 30 wt% loading.[156]

Threading a linear PIL into an MOF was further explored as an ion-exchange material, which is important in a diverse range of applications, including water purification and precious metal recovery. Conventional ion exchange resins, which consist of crosslinked polymers with a low surface area, decrease the contact efficiency between the ion-exchange sites and guest species. In the PIL–MOF composite, the polymer chains are segregated by the ordered MOF structure without entanglement, which forces full contact with solvent molecules that enter the open framework. Consequently, the composite synthesized by the fusion of poly(vinylbenzyltrimethylammonium hydroxide) into ZIF-8 facilitates fast ion exchange behavior toward nitrate ($\sim$50% in 1 min) and gold cyanide ($\sim$100% in 5 min) in solution. In comparison, a conventional ion exchange resin Amberlyst-A26 (nitrate: $\sim$50% in 60 min, gold cyanide: $\sim$100% in 30 min) bears unevenly distributed binding sites inside the resin, which are composed of cross-linked chains and a highly irregular porous structure that limits the hydrated domains (Fig. 19).[157,158]

Composites can not only accelerate adsorption kinetics but also sense toxic gas. Very recently, we developed a morphological replacement method that employed a prefabricated ionically crosslinked porous PIL membrane as a reactive

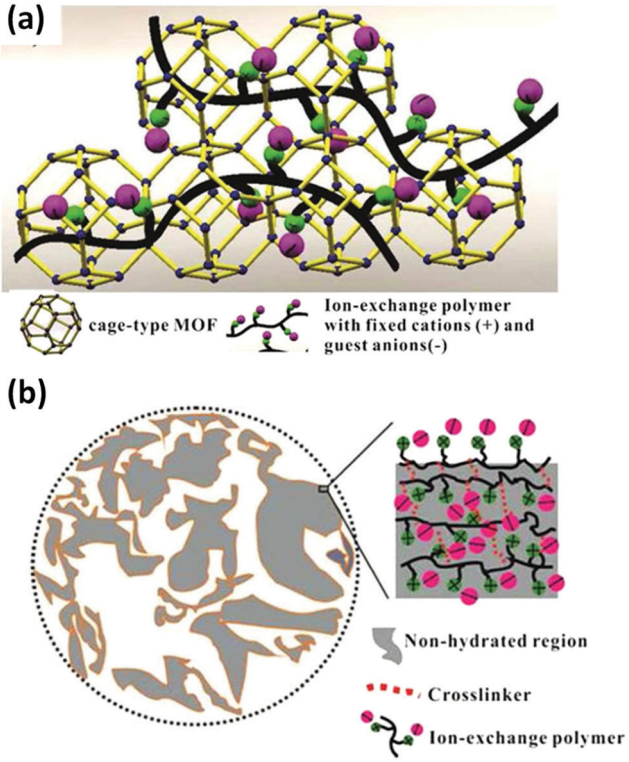


Fig. 19 Schematic illustration of the structures of the ion-exchange materials: (a) PVBTAH–ZIF-8 and (b) a microscopic view of a standard ion-exchange resin with random pore distribution, *e.g.*, Amberlyst-A26, with the majority of active sites hidden inside the nonhydrated regions of the bead. Reprinted with permission from ref. 158. Copyright 2014 American Chemical Society.

template and precursor. The *in situ* transformation from the porous PIL membrane bearing a gradient crosslinking density along its cross-section produced an asymmetric nanoporous MOF hybrid membrane that possessed a gradient size and mass distribution of MOF crystals throughout the membrane cross-section (Fig. 20a). The as-synthesized HKUST-1 hybrid membrane, due to its intrinsic asymmetric structure, could actuate at a high speed (bending curvature of 0.42 $mm^{-1}$ in 0.5 s) when in contact with $NH_3$ gas, which was the first example of MOF membrane-based actuators (Fig. 20b).[57] Such a membrane could serve as an $NH_3$ gas sensor as the curvature of the actuator was linearly proportional to the content of $NH_3$ gas.

### 4.9 PIL–biosubstance composites

A biosubstance is a material intentionally made from substances derived from living (or once-living) organisms. Recently, materials scientists have pursued hybrid or composite biosubstances to synergize the beneficial properties of multiple materials into a superior matrix. The fusion of PILs with biosubstances is an emerging method for fabricating composites with enhanced material performance.[159,160] For example, PIL membranes after being impregnated with cellulose nanofibrils had improved tensile strength up to $10^4$ MPa, which is much higher than that of commercial porous polymer filtration membranes.[161]

 

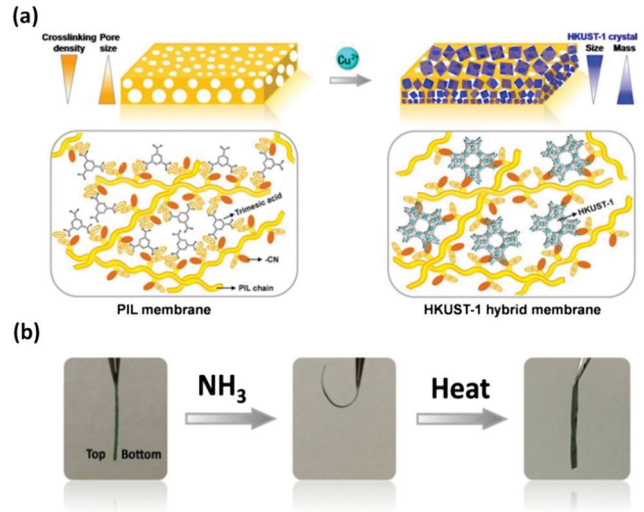


Fig. 20 (a) A schematic of the pseudomorphic replacement approach to the preparation of an asymmetric MOF (HKUST-1) hybrid membrane (right) from a porous PIL membrane (left) template and precursor. The process involves the breaking of the electrostatic ionic complexation by the coordination ions and the spontaneous formation of the HKUST-1 phase. Then, it is glued together by the leftover PIL and more locally by the cyano group (red ellipse) of the PIL polymer, which promotes integrity of the macroscopic morphology. (b) Adaptive movement of an HKUST-1 hybrid membrane (11 mm × 2 mm × 38 mm) placed in $NH_3$ gas and then back out after a heat treatment. Reprinted with permission from ref. 57. Copyright 2017 Royal Society of Chemistry.

Another example is the combination of guar gum (a plant-based polysaccharide) with an imidazolium-based PIL, which leads to a composite with tunable elasticity up to $3 \times 10^4$ Pa and a high conductivity of $>10^{-4}$ S cm$^{-1}$ at 30 °C; the above results can be attributed to intermolecular polar interactions (mainly hydrogen bonds) and a topologic chain entanglement-induced formation of physical biohybrid ionogels. This medium enables a good compromise between mechanical cohesion and ion transport.[162]

PILs can graft onto the surface of the biosubstance *via in situ* polymerization to accelerate the conversion of natural biomass into functional porous carbons, modify the surface of the biomass or endow the composites with new functions. For example, Zhang *et al.* applied PILs to improve the hydrothermal carbonization (HTC) performance of D-fructose and D-glucose to prepare porous nitrogen-doped carbon particles. The carbon products derived from pristine sugars without or with only IL additives showed a small surface area ($S_{BET}$ < 10 m$^2$ g$^{-1}$); in contrast, the use of PIL additives at weight fractions of 0.55–13.3% significantly increased $S_{BET}$ up to 572 m$^2$ g$^{-1}$. The better performance of PILs over ILs in the formation of pores was assigned to the multivalent binding power of PILs. The yield of the HTC product from pure fructose was lower than that of HTC with PIL additives, confirming the catalytic effect of PILs in accelerating the HTC process of sugars.[163] Similarly, we developed an *in situ* process to graft a PIL, poly(1-ethyl-3-vinylimidazolium TFSI), onto natural cotton. For this special morphology, the PIL coating could accelerate the activation of cotton into porous carbons even at a weight fraction as low as 3.4 wt%. During the activation process, good preservation of the microscopic fiber structure and the macroscopic morphology was achieved, and the resulting microporous carbon fibers were mechanically flexible. Such a strategy could also be extended to activate sugar-based molecules and polysaccharide biosubstances for porous carbon production.

PILs bearing abundant supramolecular interaction sites are also good for immobilizing enzymes for biocatalysts. For example, a PIL-supported B12 catalyst with a Ru(II) trisbipyridine photosensitizer ($[Ru(bpy)_3]Cl_2$) as a visible light-driven photocatalyst (B12-BVIm-Ru polymer) shows enhanced emission and a relatively high quantum yield compared to a monomer mixture in an IL due to the rigidochromic effect of the polymer.[164] Goto *et al.* encapsulated horseradish peroxidase in PIL microparticles (PIL-MP) prepared by polymerization of an IL monomer in a concentrated water-in-oil emulsion. The enzyme encapsulated in PIL-MP was chemically modified with comb-shaped polyethylene glycol-grafted molecules and showed more than twice the level of activity of an enzyme encapsulated in polyacrylamide microparticles.[165] Großeheilmann and coworkers reported that a lipase enzyme immobilized in imidazolium-based PIL hydrogels showed significantly increased activity in comparison to a nonimmobilized enzyme. Here, PIL-based hydrogels provided a good environment for lipases due to their high chemical stability and adjustable water content for folding the protein, which was responsible for the improved activity and selectivity of the enzyme. Moreover, the enzyme catalyst was easily recyclable due to the high mechanical and chemical stability of the PILs.[166]

In addition, PIL–biosubstance composites can be used in other biofields. DNA–polycation complexes are known as one of the most promising systems in gene therapy due to their salient features, such as aqueous solubility, charge neutralization, pH sensitivity, and tunable physicochemical properties. In this regard, Vijayakrishna and coworkers investigated the interaction between calf thymus DNA (ctDNA) and imidazolium-based PILs with three different alkyl side chains (ethyl, butyl, and hexyl). An increase in the binding effect between the PIL and DNA was identified when increasing the length of the alkyl side chain on the PIL, suggesting that there was a binding contribution from both hydrophobic interactions and electrostatic interactions (Fig. 21). However, if the electrostatic cohesion between the polymer and DNA is too strong for the adequate release of DNA into the cell, transfection efficiency can be dramatically suppressed. The ability to manipulate these coulombic interactions is instrumental for the optimization of transfection efficiency.[167] Campos and coworkers found that the trisaminocyclopropenium (TAC)-functionalized PIL was highly biocompatible and exhibited efficient DNA transfection. The cyclopropenium cation was stable across a broad pH range, and the resulting materials were particularly robust in utilization.[168]

### 4.10 PIL–electrode composites

ILs possessing unique electrochemical characteristics, such as large electrochemical windows and high ion conductivity, have been proposed in several electrochemical applications,

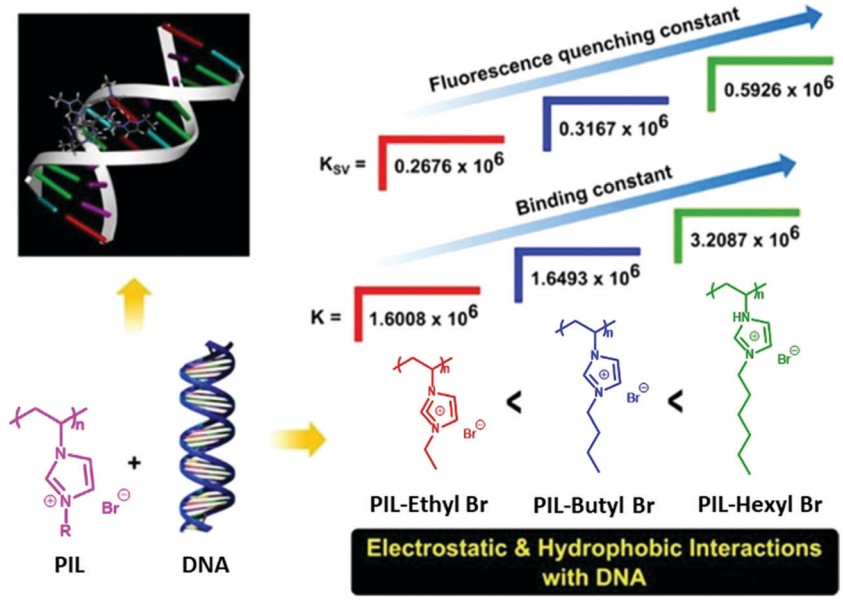


Fig. 21 Comparison of binding between DNA and PILs bearing different alkyl side chains. Reprinted with permission from ref. 167. Copyright 2015 American Chemical Society.

including electrochemical capacitors, lithium-ion batteries, fuel cells, and solar batteries. PILs inherit the properties of both ILs and polymer chains. This combination allows a new class of polymeric materials to be engineered as new polymer electrolytes for use in energy, environment, and catalysis applications. In addition, PILs can also be grafted onto traditional electrodes to form new composite electrodes that have an improved accessibility for electrolyte ions at the electrode surface. Randriamahazaka and coworkers deposited a redox-active PIL poly(3-(2-methacryloyloxyethyl)-1-ferrocenylmethylimidazolium TFSI) (poly[MAEImMFc][TFSI]) onto gold electrode surfaces *via* an SI-ATRP technique. The electrochemical characterization of the PIL-modified electrode in electrolytic acetonitrile solution showed the presence of a reversible redox signal that was characteristic of surface-confined electroactive layers. Ferrocenyl PIL-modified electrodes have been used as reversible redox-responsive materials because the reversible wettability of the polymer can be electrochemically switched on/off. In addition, the redox PILs exhibited electrocatalytic activity and a voltammetric response toward tyrosine.[76]

To date, the development of PILs for electrolyte applications has mainly focused on PILs carrying a TFSI anion because of their highly delocalized charge distribution and excellent plasticizing effect, as well as good compatibility with various electrodes, such as Li metal. To develop better PIL-based solid polymer electrolytes (SPEs), Nie and coworkers prepared an SPE comprised of poly[*N*,*N*-dimethyl-*N*-[2-(methacryloyloxy)ethyl]-*N*-[2-(2-methoxyethoxy)ethyl]ammonium] ($P[C_5O_2N_{MA,11}]$) and LiFSI. It was demonstrated that the ion conductivity of the LiFSI/$P[C_5O_2N_{MA,11}]$FSI electrolyte was higher than that of the corresponding TFSI-based electrolyte. The interfacial resistances of the Li symmetric cell (Li metal|polymer electrolytes|Li metal) using the LiFSI/$P[C_5O_2N_{MA,11}]$FSI electrolyte were much lower than those using the LiTFSI/$P[C_5O_2N_{MA,11}]$TFSI electrolyte. Additionally, the FSI anion displayed a better plasticizing effect than the TFSI anion, which reduced the $T_g$ and increased the ionic conductivity of the polymer electrolytes.[169]

PILs have also been explored as binders in batteries. Our group has pioneered the use of imidazolium-based PILs for binder applications.[170] Paillard and coworkers synthesized cross-linked PIL NPs by dispersion polymerization of 1-vinyl-3-ethylimidazolium TFSI; the above material was used as a binder for Li-ion battery electrodes that were based on graphite microparticles and carbon-coated submicrometric $Li_4Ti_5O_{12}$ (LTO) particles. The graphite/PIL NP electrodes were cycled for more than 7 months, and the LTO/PIL NP electrodes provided excellent capacities, rate performances and long-term cycling stability. The excellent binding properties of the nanolatex resulted from the reduction of the PIL at low potentials, leading to chemical bonding of the binder to the carbon surface. Additionally, the use of an insoluble binder strongly reduced electrode cracking or exfoliation from the current collectors, which can be caused by a soluble binder retracting upon drying.[171]

Similarly, PIL binders possessing different chemical structures, polymer backbones, and polymeric architectures, including linear homopolymers and nanoparticles, have been used as cathode binders in lithium–sulfur batteries. In all cases, the PILs are generally better than the commercial benchmark binder PVDF with respect to cyclability and discharge capacities in extended cycling experiments. The improvement is ascribed to the better compatibility between the PILs and the produced sulfides, which inhibits swelling-induced degradation and retention of the sulfides within the cathode. PIL binders mixed with sulfide species result in more uniformly distributed sulfides in the cathode and better sulfide transport. These features help to

 

mitigate the volume change-induced degradation of electrodes that typically plague Li–S batteries. The uptake of polysulfides by PILs also inhibits the polysulfide shuttling effect during battery cycling, leading to better cycling stability.[172]

Helms and coworkers highlighted at a molecular level the importance of macromolecular design and mechanistic understanding of PIL binders in the development of Li–S battery technology. PDADMA–TFSI (denoted as PEB-1) was shown to both facilitate $Li^+$ transport through its reconfigurable network of mobile anions and restrict polysulfide diffusion from mesoporous carbon hosts by anion metathesis. Cells carrying such a PIL binder exhibited excellent rate capability (>100 cycles) using cathodes with areal sulfur loadings up to 8.1 mg $cm^{-2}$. For comparison, composite sulfur cathodes with a PVDF binder exhibited slower and more rapidly degrading electrode kinetics (Fig. 22).[173]

### 4.11 PIL–IL composites

ILs can mix smoothly with PILs to engineer functional PIL–IL composites. One advantage of such composites is their enhanced ionic conductivity in comparison with sole PILs, which are potential candidates as quasi-solid electrolytes in energy conversion and storage devices. PILs in a solid-state normally suffer from limited mobility of the ionic backbone that can be considered to be in a frozen state, and thus only the counteranions serve as mobile charge carriers. The PIL–IL composite may carry the synergy of ILs to increase the number of charge carriers and of PILs for the needed mechanical strength of the electrolyte to reduce the recurring problem of incompatibility between the ILs and other host polymers.[174–178] For example, in an imidazolium-based PIL/IL gel system, increasing the free IL content from 50 to 80 wt% produced an ion conductor with conductivity values $\geq 10^{-2}$ S $cm^{-1}$ at 25 °C and $\approx 10^{-1}$ S $cm^{-1}$ at 110 °C.[176] Oliveira *et al.* developed a type of gel electrolyte by mixing a PIL matrix and two ILs, namely, 1-methyl-3-butylimidazolium bis(fluorosulfonyl)imide (MBIMFSI) and 1,2-dimethyl-3-propylimidazolium TFSI (DPITFSI), as a quasi-solid-state electrolyte for use in supercapacitors.[178] The synthesized PIL/IL gel electrolyte exhibited an ion conductivity as high as $3.2 \times 10^{-3}$ S $cm^{-1}$ at 25 °C and an electrochemical window of 2.8 V (obtained by linear sweep voltammetry). The corresponding supercapacitor devices showed a specific capacitance of 49.1 F $g^{-1}$ and 41.2 F $g^{-1}$ at the positive and negative electrodes, respectively, as well as a satisfactory energy density (9.8 W h $kg^{-1}$) and power density (532 W $kg^{-1}$) at 0.5 A $g^{-1}$ and 2.5 V. On the basis of these achievements, by a judicious choice of the PIL matrix and suitable ILs as well as the optimized composite fabrication method, PIL/IL composites may play a more crucial role in the current pursuit of high-safety energy conversion and storage devices.

In addition to being used as quasi-solid electrolytes, PIL–IL composites have great potential to serve as MMMs for gas separation, *e.g.*, $CO_2/N_2$ or $CO_2/CH_4$. Despite the fact that PILs provide an alternative choice to design IL-based membrane materials for $CO_2$ separation, the relatively low gas permeability and diffusivity of neat PIL membranes forces researchers instead to develop PIL/IL composite membranes. The aim is to combine their particular features together for enhanced $CO_2$ transport properties.[179–183] In a PIL/IL composite membrane, the PIL provides the necessary mechanical stability while the IL secures a high gas permeability and diffusivity. Noble and Gin

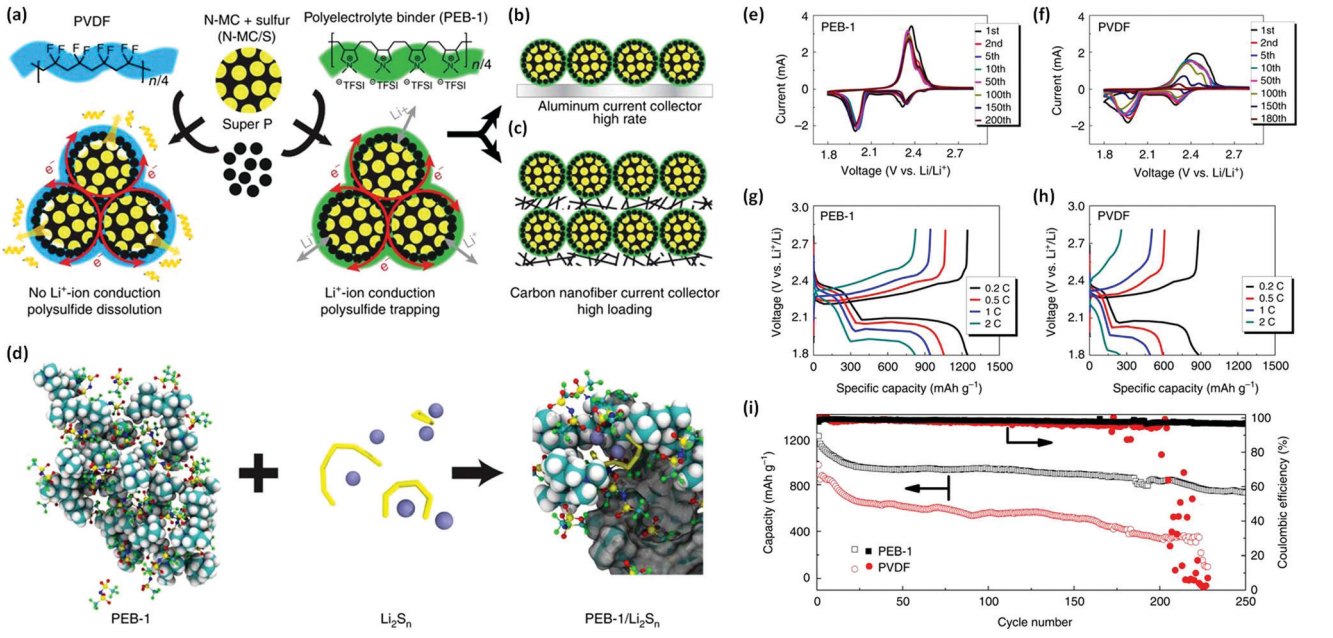


Fig. 22 (a) Illustration showing the fabrication of sulfur electrodes with a PVDF or PEB-1 binder. (b) A conventional sulfur cathode and (c) a highly loaded sulfur cathode cast onto an aluminum current collector. (d) Schematic illustrating the formation of complex ion clusters *via* anion metathesis. (e and f) Long-term cyclic voltammetry (CV). (g and h) Discharge and charge curves at different C rates. (i) Cycling performance for each cell type at a rate of C/5. Reprinted with permission from ref. 173. Copyright 2017 Nature Publishing Group.

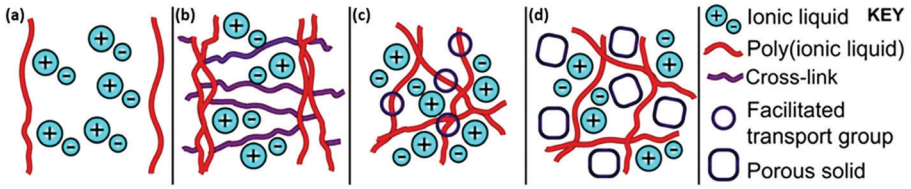


Fig. 23 A series of PIL/IL ion-gel membranes were developed by Noble and Gin *et al.* (a) A linear PIL/IL ion-gel system in a composite membrane; (b) cross-linked PIL/IL ion-gel materials with improved $CO_2$ permeability; (c) PIL/IL ion-gels that incorporate facilitated transport groups to improve $CO_2$ permeability and $CO_2/N_2$ separation selectivity; and (d) MMMs that incorporate a microporous solid with improved $CO_2$ permeability and $CO_2$/light gas selectivity. Reprinted with permission from ref. 179. Copyright 2016 American Chemical Society.

*et al.* have carried out pioneering work in this area (Fig. 23). The proof-of-concept for PIL/IL composite membranes for gas separation was reported in 2008.[184] Over the past few years, their systematic studies include the preparation of PIL/IL composites and their use as high-performance, ultrathin selective layers in composite membranes for $CO_2/N_2$ separation. For example, 100-nm-thick active layers were produced for high-performance composite membranes with $CO_2$ permeance $\geq$6000 GPU (gas permeation units) and an ideal $CO_2/N_2$ selectivity of approximately 22. The detailed work has been summarized in a recent and brief review by Noble, Gin and coworkers.[179] In fact, the addition of free ILs increases the $CO_2$ permeability of PIL/IL membranes, and the gas permeation properties of the free IL significantly influence the $CO_2$ separation performance of the composites. Consequently, the choice of an appropriate IL is crucial in tailoring the PIL/IL membrane performance in $CO_2$ separation. Marrucho,[183] Chung,[185] and other researchers have also contributed significantly to this area, which can be referred to in the recent comprehensive review article.[182]

In addition to the above-mentioned extensively explored methods for $CO_2$ separation from flue or other similar gases, PIL/IL composite membranes can also be used for $CO_2/H_2$ separation. In particular, the implementation of high-performance and cost-effective biohydrogen (bio$H_2$) purification techniques is of vital importance, especially for fuel cell applications.[186,187] Carlisle *et al.* explored $CO_2/H_2$ separation through imidazolium-based PIL/IL gel membranes produced by UV-initiated polymerization.[186] The time-lag experiments performed at room temperature and 200 kPa of feed pressure showed an ideal $CO_2/H_2$ selectivity ranging from 6.6 to 12 for membranes prepared with 5 to 100 mol% of a cross-linking monomer and different amounts of an IL monomer. Their optimized composite system, containing 100 mol% cross-linking monomer and 75 wt% IL, showed a $CO_2$ permeability of 540 barrer and a $CO_2/H_2$ selectivity of 12. Marrucho's group used pyrrolidinium-based PILs with $[C(CN)_3]^-$ or $[NTf_2]^-$ anions and different amounts of ILs ($[C_2mim][C(CN)_3]$, $[C_4mpyr][NTf_2]$ or $[C_2mim][NTf_2]$) incorporated into the $CO_2/H_2$ separation membranes. Particularly at 308 K, the PIL $C(CN)_3$–60 IL $C(CN)_3$ composite membrane delivered a $CO_2$ permeability of 505 barrer and a $CO_2/H_2$ selectivity of 12.5.[188]

### 4.12 PIL–other composites

In addition to the PIL-based composites mentioned above, PILs have been explored in combination with other materials to produce composites with intriguing structures and improved performance in catalysis, separation, and sensing.

PILs were shown to be important elements for fabricating membranes as separators and sensors. For example, *via* solvothermal copolymerization of an IL monomer 1-ethyl-3-vinylimidazolium bromide (EVImBr) and divinylbenzene (DVB) inside a tissue paper as a template, a polymer-paper hybrid membrane bearing high porosity and mechanical flexibility was fabricated.[9] The hybrid membrane is porous, and the surface area is dependent on the weight fraction of the copolymer impregnated inside the tissue paper. The as-synthesized composite membrane shows controlled surface wettability in terms of ethanol wetting and vacuum drying, endowing the membrane with a switchable oil/water separation function.

When combined with biological templates, PILs were able to replicate and preserve complicated and inherent structural motifs of the templates at a micro- to macroscale due to the advantages of their high surface activity, their reaction with the carbohydrate template and their resulting oxidative stability. We functionalized *Hoplia coerulea* beetles with a PIL layer on their surface, followed by a low temperature calcination under nitrogen to maintain the surface morphology at the microscale.[189] In this process, the thin PIL coating layer bearing a dicyanamide (DCA) anion provided precise microstructure preservation. The DCA anions built up cross-linking points at elevated temperature, thus stabilizing the scale morphology since DCA is known to undergo a trimerization-type crosslinking reaction, which forms triazine networks and reduces the structural fragmentation at elevated temperature.

Structurally well-defined and tailored PILs provide the ability to reach a low $T_g$ and promote a high chain mobility, which increase ion conductivity. However, the weak intermolecular interactions of PILs result in poor mechanical cohesion, limiting their applicability. To solve this problem, Walther and coworkers combined the mechanical design principles of nacre-mimetics with the ion conductive nature of a PIL, poly(1-ethyl-3-vinylimidazolium dicyanamide), resulting in nanoplatelets bearing a core–shell structure.[190] PILs were adsorbed onto the anionic basal planes of the nanoclay due to electrostatic complexation as well as hydrophobic and van der Waals interactions. The as-prepared nanocomposites showed attractive multifunctional property profiles with high transparency, satisfactory values of ion conductivity, and high stiffness and strength.

 

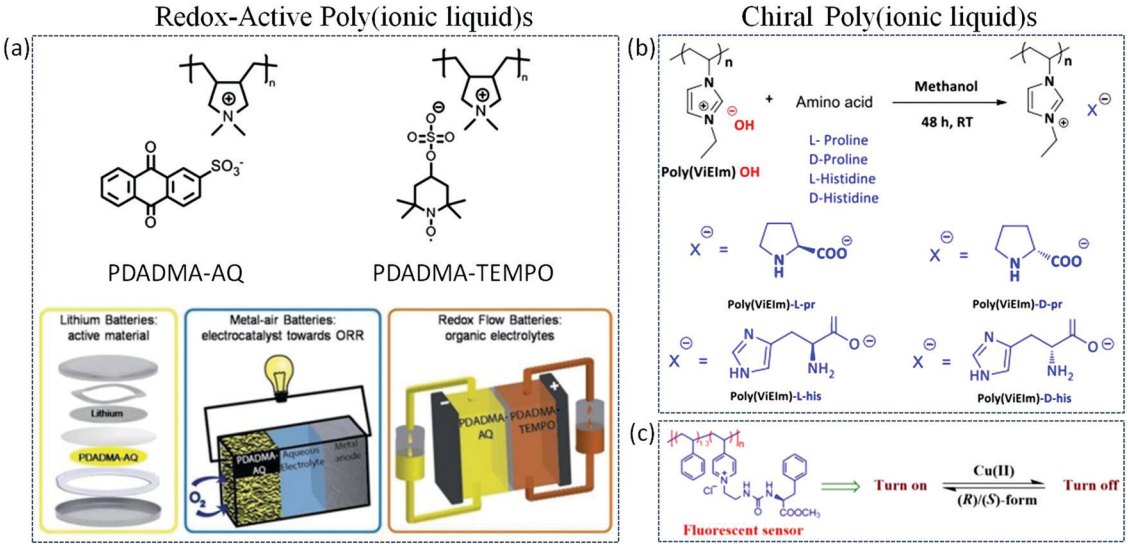


Fig. 24 A selection of emerging and new functional PIL candidates for composite preparation. Reprinted with permission from ref. 191–193. Copyright 2017 Royal Society of Chemistry and 2018 American Chemical Society.

## 5. Conclusion and perspective

Upon the ongoing exploration of new PIL chemical structures, PIL-based materials chemistry has entered a very exciting era. Chemists now have expanded beyond the synthesis and structural characterization of new PILs, and more efforts will be made to integrate PILs into useful materials that tackle problems and challenges in life science, energy, environment, *etc.*

This review article has described the synthetic methodologies for PIL composites, as well as the fascinating properties of the hybrid materials. The integration of PILs into different substances has provided unique aspects in composites, especially the synergistic effects that arise from each component. Nevertheless, the development of PIL composites is still in its infancy. Although some structures have been synthesized, dedicated integration of PILs with more functions is highly desirable for further development in terms of materials chemistry. For example, Mecerreye and coworkers recently incorporated organic redox moieties such as nitroxide 2,2,6,6-tetramethylpiperidine-1-oxyl (TEMPO) or anthraquinone (AQ) derivatives as counteranions into PDADMA-type PILs. This new family of redox-active PILs can be applied in several electrochemical energy storage technologies, such as lithium batteries, as electrocatalysts in fuel cells and metal–air batteries or as electrolytes in organic redox flow batteries (Fig. 24a).[191] Another example is the introduction of chiral moieties into PILs, which can be used as fluorescence off/on sensors for chiral recognition or asymmetric catalytic applications (Fig. 24b).[192,193] These emerging examples highlight a promising way to engineer diverse functional PILs (*e.g.*, conductivity) for composite fabrication and applications.

Currently, most of the studies on PIL composites focus on metal nanostructured materials or carbons, and the resultant composites have already shown enhanced electric, thermal and mechanical properties, which outperform traditional materials. These advantages arise from the periodic arrangement of ILs, and the ion conductivity, electrochemical stability and processability; furthermore, the high compatibility of PILs with substances based on multiple interactions and synergetic effects also provide advantages. However, there is considerable room to explore new functions and materials, especially using PILs in combination with emerging nanoporous materials such as MOFs, COFs, or bio-substances. In this regard, intriguing nanostructured composites with hierarchical architectures and fantastic properties, such as host–guest synergistic functions and heterogeneous biocatalysis with high efficiency, can be expected and represent an exciting area of great opportunity.

Further investigation of novel PIL composite materials is also closely dependent on a better understanding of structure–property relationships and physicochemical behaviors. In most reported PIL composites, an active interplay between the PIL and the other substance can be identified. A better understanding of the mechanism, especially the heterojunction effect derived from a biphase between PIL and substance, will undoubtedly help judicious design and improve the value of the composite materials. This knowledge will inspire ideas and catalyze more directions to harness the PIL family to a wider scope of composites.

## Conflicts of interest

There are no conflicts of interest to declare.

## Acknowledgements

J. K. S. acknowledges Starting Grant from Beijing Institute of Technology (3100011181910). J. Y. is grateful for financial support from the ERC Starting Grant NAPOLI-639720 from European Research Council, Stockholm University Strategic

fund, Swedish Research Council grant 2018-05351, Dozentenpreis 15126 from Verband der Chemischen Industrie e.V. (VCI) in Germany, and the Wallenberg Academy Fellow program (KAW 2017.0166) in Sweden. Q. Z. acknowledges the funding from National Natural Science Foundation of China (Grant No. 21703172) and the Fundamental Research Funds for the Central Universities (Grant No. 310201911cx043).

## References

1 J. Yuan and M. Antonietti, *Polymer*, 2011, **52**, 1469–1482.
2 J. Yuan, D. Mecerreyes and M. Antonietti, *Prog. Polym. Sci.*, 2013, **38**, 1009–1036.
3 J. Lu, F. Yan and J. Texter, *Prog. Polym. Sci.*, 2009, **34**, 431–448.
4 D. Mecerreyes, *Prog. Polym. Sci.*, 2011, **36**, 1629–1648.
5 W. Qian, J. Texter and F. Yan, *Chem. Soc. Rev.*, 2017, **46**, 1124–1159.
6 J. Gong, H. Lin, J. W. C. Dunlop and J. Yuan, *Adv. Mater.*, 2017, **29**, 1605103.
7 P. Kallem, A. Eguizabal, R. Mallada and M. P. Pina, *ACS Appl. Mater. Interfaces*, 2016, **8**, 35377–35389.
8 P. Zhang, M. Li, B. Yang, Y. Fang, X. Jiang, G. M. Veith, X. G. Sun and S. Dai, *Adv. Mater.*, 2015, **27**, 8088–8094.
9 C. X. Cao, J. Yuan, J. P. Cheng and B. H. Han, *Sci. Rep.*, 2017, **7**, 3101.
10 R. Lambert, A. L. Wirotius, J. Vignolle and D. Taton, *Polym. Chem.*, 2019, **10**, 460–466.
11 R. Lambert, A. L. Wirotius, S. Garmendia, P. Berto, J. Vignolle and D. Taton, *Polym. Chem.*, 2018, **9**, 3199–3204.
12 S. Chen, Y. Xiang, M. K. Banks, C. Peng, W. Xu and R. Wu, *Nanoscale*, 2018, **10**, 20043–20052.
13 W. Bi, M. Tian and K. H. Row, *Analyst*, 2012, **137**, 2017–2020.
14 K. Täuber, Q. Zhao, M. Antonietti and J. Yuan, *ACS Macro Lett.*, 2015, **4**, 139–142.
15 H. Du, X. Liu, Y. Yu, Y. Xu, Y. Wang and Z. Liang, *Macromol. Chem. Phys.*, 2016, **217**, 2626–2634.
16 Z. Li, W. Wang, Y. Chen, C. Xiong, G. He, Y. Cao, H. Wu, M. D. Guiver and Z. Jiang, *J. Mater. Chem. A*, 2016, **4**, 2340–2348.
17 J. Gong, M. Antonietti and J. Yuan, *Angew. Chem., Int. Ed.*, 2017, **56**, 7557–7563.
18 D. Ager, V. A. Vasantha, R. Crombez and J. Texter, *ACS Nano*, 2014, **8**, 11191–11205.
19 I. K. Oh, J. H. Jung, J. H. Jeon and S. Vadahanambi, *Smart Mater. Struct.*, 2010, **19**, 075009.
20 G. Choi, G. M. Jeong, M. S. Oh, M. Joo, S. G. Im, K. J. Jeong and E. Lee, *ACS Biomater. Sci. Eng.*, 2018, **4**, 2614–2622.
21 M. G. Cowan, D. L. Gin and R. D. Noble, *Acc. Chem. Res.*, 2016, **49**, 724–732.
22 R. Gao, D. Wang, J. R. Heflin and T. E. Long, *J. Mater. Chem.*, 2012, **22**, 13473–13476.
23 M. H. Yang, B. G. Choi, S. C. Jung, Y. K. Han, Y. S. Huh and S. B. Lee, *Adv. Funct. Mater.*, 2014, **24**, 7301–7309.
24 T. T. Tung, C. Pham-Huu, I. Janowska, T. Y. Kim, M. Castro and J. F. Feller, *Small*, 2015, **11**, 3485–3493.
25 C. P. Lee and K. C. Ho, *Eur. Polym. J.*, 2018, **108**, 420–428.
26 R. Marcilla, J. A. Blazquez, J. Rodriguez, J. A. Pomposo and D. Mecerreyes, *J. Polym. Sci., Part A: Polym. Chem.*, 2004, **42**, 208–212.
27 Y. Ye and Y. A. Elabd, *Macromolecules*, 2011, **44**, 8494–8503.
28 J. Pinaud, J. Vignolle, Y. Gnanou and D. Taton, *Macromolecules*, 2011, **44**, 1900–1908.
29 C. Huang, X. Qian and R. Yang, *Mater. Sci. Eng., R*, 2018, **132**, 1–22.
30 A. Shaplov, D. Ponkratov and Y. Vygodskii, *Polym. Sci., Ser. B*, 2016, **58**, 73–142.
31 Y. Ye and Y. A. Elabd, *Polymer*, 2011, **52**, 1309–1317.
32 R. Marcilla, J. A. Blazquez, R. Fernandez, H. Grande, J. A. Pomposo and D. Mecerreyes, *Macromol. Chem. Phys.*, 2005, **206**, 299–304.
33 J. Yuan, S. Prescher, K. Sakaushi and M. Antonietti, *J. Mater. Chem. A*, 2015, **3**, 7229–7234.
34 H. Ohno, Design of ion conductive polymers based on ionic liquids, *Macromol. Symp.*, 2007, 551–556.
35 W. Ogihara, S. Washiro, H. Nakajima and H. Ohno, *Electrochim. Acta*, 2006, **51**, 2614–2619.
36 M. Yoshizawa and H. Ohno, *Chem. Lett.*, 1999, 889–890.
37 H. Chen, J.-H. Choi, D. Salas-de la Cruz, K. I. Winey and Y. A. Elabd, *Macromolecules*, 2009, **42**, 4809–4816.
38 H. Hu, W. Yuan, L. Lu, H. Zhao, Z. Jia and G. L. Baker, *J. Polym. Sci., Part A: Polym. Chem.*, 2014, **52**, 2104–2110.
39 S. Washiro, M. Yoshizawa, H. Nakajima and H. Ohno, *Polymer*, 2004, **45**, 1577–1582.
40 R. L. Weber, Y. Ye, S. M. Banik, Y. A. Elabd, M. A. Hickner and M. K. Mahanthappa, *J. Polym. Sci., Part B: Polym. Phys.*, 2011, **49**, 1287–1296.
41 G. Appetecchi, G.-T. Kim, M. Montanino, M. Carewska, R. Marcilla, D. Mecerreyes and I. De Meatza, *J. Power Sources*, 2010, **195**, 3668–3675.
42 M. Hayyan, F. S. Mjalli, M. A. Hashim, I. M. AlNashef and T. X. Mei, *J. Ind. Eng. Chem.*, 2013, **19**, 106–112.
43 G. G. Eshetu, D. Mecerreyes, M. Forsyth, H. Zhang and M. Armand, *Mol. Syst. Des. Eng.*, 2019, **4**, 294–309.
44 A. L. Pont, R. Marcilla, I. De Meatza, H. Grande and D. Mecerreyes, *J. Power Sources*, 2009, **188**, 558–563.
45 R. Marcilla, M. L. Curri, P. D. Cozzoli, M. T. Martínez, I. Loinaz, H. Grande, J. A. Pomposo and D. Mecerreyes, *Small*, 2006, **2**, 507–512.
46 M. Antonietti, Y. Shen, T. Nakanishi, M. Manuelian, R. Campbell, L. Gwee, Y. A. Elabd, N. Tambe, R. Crombez and J. Texter, *ACS Appl. Mater. Interfaces*, 2010, **23**, 649–653.
47 J. Texter, R. Crombez, R. Maniglia, X. Ma, V. Arjunan, V. M. Manuelian, R. Campbell, L. Slater and T. Mourey, *J. Surfactants Deterg.*, 2019, **22**, 1059–1071.
48 R. Marcilla, E. Ochoteco, C. Pozo-Gonzalo, H. Grande, J. A. Pomposo and D. Mecerreyes, *Macromol. Rapid Commun.*, 2005, **26**, 1122–1126.

49 T. Kim, M. Suh, S. J. Kwon, T. H. Lee, J. E. Kim, Y. J. Lee, J. H. Kim, M. Hong and K. S. Suh, *Macromol. Rapid Commun.*, 2009, **30**, 1477–1482.
50 T. Kim, H. Lee, J. E. Kim and K. S. Suh, *ACS Nano*, 2010, **4**, 1612–1618.
51 T. Y. Kim, H. W. Lee, M. Stoller, D. R. Dreyer, C. W. Bielawski, R. S. Ruoff and K. S. Suh, *ACS Nano*, 2011, **5**, 436–442.
52 J. K. Sun, M. Antonietti and J. Yuan, *Chem. Soc. Rev.*, 2016, **45**, 6627–6656.
53 X. Li, K. Wang, N. Ma and X. Jia, *Front. Chem.*, 2017, **5**, 69.
54 M. R. Gao, S. H. Yu, J. Yuan, W. Zhang and M. Antonietti, *Angew. Chem., Int. Ed.*, 2016, **55**, 12812–12816.
55 J. K. Sun, Z. Kochovski, W. Zhang, H. Kirmse, Y. Lu, M. Antonietti and J. Yuan, *J. Am. Chem. Soc.*, 2017, **139**, 8971–8976.
56 X. He, W. Yang and X. Pei, *Macromolecules*, 2008, **411**, 34615–34621.
57 J. K. Sun, H. J. Lin, W. Y. Zhang, M. R. Gao, M. Antonietti and J. Yuan, *Mater. Horiz.*, 2017, **4**, 681–687.
58 K. Ahmed, A. Khosla and H. Furukawa, *Nanosensors, Biosensors, Info-tech Sensors & 3d Systems*, 2017.
59 L. Y. Chang, C. P. Lee, C. T. Li, M. H. Yeh, K. C. Ho and J. J. Lin, *J. Mater. Chem. A*, 2014, **2**, 20814–20822.
60 Z. Zheng, J. Guo, H. Mao, Q. Xu, J. Qin and F. Yan, *ACS Biomater. Sci. Eng.*, 2017, **3**, 922–928.
61 H. Li, Q. Zhang, X. Liu, F. Chang, Y. Zhang, W. Xue and S. Yang, *Bioresour. Technol.*, 2013, **144**, 21–27.
62 R. N. Biboum, F. Doungmene, B. Keita, P. D. Oliveira, L. Nadjo, B. Lepoittevin, P. Roger, F. Brisset, P. Mialane and A. Dolbecq, *J. Mater. Chem.*, 2011, **22**, 319–323.
63 Q. Zhao, S. Soll, M. Antonietti and J. Yuan, *Polym. Chem.*, 2013, **4**, 2432–2435.
64 Q. Zhao, M. Yin, A. P. Zhang, S. Prescher, M. Antonietti and J. Yuan, *J. Am. Chem. Soc.*, 2013, **135**, 155549.
65 B. Zhang, G. Sudre, G. Quintard, A. Serghei, L. David, J. Bernard, E. Fleury and A. Charlot, *Carbohydr. Polym.*, 2017, **157**, 586–595.
66 S. Amajjahe and H. Ritter, *Macromolecules*, 2008, **41**, 3250–3253.
67 A. Panniello, C. Ingrosso, P. Coupillaud, M. Tamborra and M. Striccoli, *Materials*, 2014, **7**, 591–610.
68 X. Li, Z. Zhang, S. Li, K. Yang and L. Yang, *J. Mater. Chem. A*, 2017, **5**, 21362–21369.
69 M. Brinkkötter, E. I. Lozinskaya, D. O. Ponkratov, P. S. Vlasov, M. P. Rosenwinkel, I. A. Malyshkina, Y. Vygodskii, A. S. Shaplov and M. Schönhoff, *Electrochim. Acta*, 2017, **237**, 237–247.
70 L. C. Tomé, D. Mecerreyes, C. S. R. Freire, L. P. N. Rebelo and I. M. Marrucho, *J. Mater. Chem. A*, 2014, **2**, 5631–5639.
71 J. F. Olorunyomi, K. Y. Chan, L. Gao, A. Voskanyan and C. Y. V. Li, *Microporous Mesoporous Mater.*, 2018, **259**, 255–263.
72 Q. Sun, Y. Tang, B. Aguila, S. Wang, F. S. Xiao, P. K. Thallapally, A. M. Al-Enizi, A. Nafady and S. Ma, *Angew. Chem., Int. Ed.*, 2019, **58**, 8670–8675.
73 D. Zhou, R. Liu, J. Zhang, X. Qi, Y. B. He, B. Li, Q. H. Yang, Y. S. Hu and F. Kang, *Nano Energy*, 2017, **33**, 45–54.
74 Y. Jiang, J. L. Freyer, P. Cotanda, S. D. Brucks, K. L. Killops, J. S. Bandar, C. Torsitano, N. P. Balsara, T. H. Lambert and L. M. Campos, *Nat. Commun.*, 2015, **6**, 5950.
75 R. Luo, Y. Chen, Q. He, X. Lin, Q. Xu, X. He, W. Zhang, X. Zhou and H. Ji, *ChemSusChem*, 2017, **10**, 1526–1533.
76 V. Bui-Thi-Tuyet, G. Trippé-Allard, J. Ghilane and H. Randriamahazaka, *ACS Appl. Mater. Interfaces*, 2016, **8**, 28316–28324.
77 X. He, Y. Wu and X. Pei, *Macromolecules*, 2008, **41**, 4615–4621.
78 W. Jia, Y. Wu, H. Jing, A. Qi, X. Dan, Y. Wu, F. Li and G. Li, *J. Mater. Chem.*, 2010, **20**, 8617–8623.
79 P. Wang, Y. N. Zhou, J. S. Luo and Z. H. Luo, *Polym. Chem.*, 2013, **5**, 882–891.
80 C. Hua, W. Ping, J. Luo, J. Fransaer, D. E. D. Vos and Z. H. Luo, *Ind. Eng. Chem. Res.*, 2015, **54**, 3107–3115.
81 J. W. Liu, M. M. Wang, Y. Zhang, L. Han, X. W. Chen and J. H. Wang, *RSC Adv.*, 2014, **4**, 61936–61943.
82 J. Liu, Y. Liang, J. Shen and Q. Bai, *Anal. Bioanal. Chem.*, 2018, **410**, 573–584.
83 L. Mao, Y. Li, C. Chi, H. SzeOn Chan and J. Wu, *Nano Energy*, 2014, **6**, 119–128.
84 R. Zhang, S. Ji, N. Wang, L. Wang, G. Zhang and J. R. Li, *Angew. Chem., Int. Ed.*, 2014, **53**, 9775–9779.
85 X. Mu, J. Meng, Z. C. Li and Y. Kou, *J. Am. Chem. Soc.*, 2005, **127**, 9694–9695.
86 A. Dani, V. Crocellà, L. Maddalena, C. Barolo and E. Groppo, *J. Phys. Chem. C*, 2016, **120**, 1683–1692.
87 S. Doherty, J. G. Knight, T. Backhouse, E. Abood, H. Al-Shaikh, A. R. Clemmet, J. R. Ellison, R. A. Bourne, T. W. Chamberlain and R. Stones, *Adv. Synth. Catal.*, 2018, **360**, 3716–3731.
88 Y. Yang, M. Ambrogi, H. Kirmse, Y. Men, M. Antonietti and J. Yuan, *Chem. Mater.*, 2015, **27**, 127–132.
89 P. Zhang, Z. A. Qiao, X. Jiang, G. M. Veith and S. Dai, *Nano Lett.*, 2015, **15**, 823–828.
90 H. Fang, S. Sun, P. Liao, Y. Hu and J. Zhang, *J. Mater. Chem. A*, 2018, **6**, 2115–2121.
91 S. Montolio, C. Vicent, V. Aseyev, I. Alfonso, M. Isabel Burguete, H. Tenhu, E. García-Verdugo and S. V. Luis, *ACS Catal.*, 2016, **6**, 7230–7237.
92 S. Prescher, F. Polzer, Y. Yang, M. Siebenbürger, M. Ballauff and J. Yuan, *J. Am. Chem. Soc.*, 2014, **136**, 12–15.
93 K. T. Prabhu Charan, N. Pothanagandhi, K. Vijayakrishna, A. Sivaramakrishna, D. Mecerreyes and B. Sreedhar, *Eur. Polym. J.*, 2014, **60**, 114–122.
94 S. Ghasemi and Z. A. Harandi, *RSC Adv.*, 2018, **8**, 14570–14578.
95 D. Batra, S. Seifert, L. M. Varela, A. C. Y. Liu and M. A. Firestone, *Adv. Funct. Mater.*, 2007, **17**, 1279–1287.
96 Y. Lu, H. Zhu, W.-J. Wang, B. G. Li and S. Zhu, *ACS Sustainable Chem. Eng.*, 2017, **5**, 2829–2835.
97 R. Zhang, P. Su, L. Yang and Y. Yang, *J. Sep. Sci.*, 2014, **37**, 1503–1510.

98 L. Yang, P. Su, X. Chen, R. Zhang and Y. Yang, *Anal. Methods*, 2015, **7**, 3246–3252.
99 H. Han, T. Jiang, T. Wu, D. Yang and B. Han, *ChemCatChem*, 2015, **7**, 3526–3532.
100 L. Zhang, J. Du, T. Ran, H. Gao and Y. Liao, *J. Mater. Sci.*, 2016, **51**, 7186–7198.
101 X. Chen, Q. Li, J. Zhao, L. Qiu, Y. Zhang, B. Sun and F. Yan, *J. Power Sources*, 2012, **207**, 216–221.
102 C. Willa, J. Yuan, M. Niederberger and D. Koziej, *Adv. Funct. Mater.*, 2015, **25**, 2537–2542.
103 C. Wang, X. Ye, Z. Wang, T. Wu, Y. Wang and C. Li, *Anal. Chem.*, 2017, **89**, 12391–12398.
104 B. Wu, D. Hu, Y. Kuang, B. Liu, X. Zhang and J. Chen, *Angew. Chem., Int. Ed.*, 2009, **48**, 4751–4754.
105 Y. Ding, A. Klyushin, X. Huang, T. Jones, D. Teschner, F. Girgsdies, T. Rodenas, R. Schlögl and S. Heumann, *Angew. Chem., Int. Ed.*, 2018, **57**, 3514–3518.
106 N. Patil, M. Aqil, A. Aqil, F. Ouhib, R. Marcilla, A. Minoia, R. Lazzaroni, C. Jerôme and C. Detrembleur, *Chem. Mater.*, 2018, **30**, 5831–5835.
107 K. Ahmed, A. Khosla, M. Kawakami and H. Furukawa, *Nanosensors, Biosensors, Info-tech Sensors & 3d Systems*, 2017.
108 D. Gendron, A. Ansaldo, G. Bubak, L. Ceseracciu, G. Vamvounis and D. Ricci, *Compos. Sci. Technol.*, 2015, **117**, 364–370.
109 H. Lin, J. Gong, M. Eder, R. Schuetz, H. Peng, J. W. C. Dunlop and J. Yuan, *Adv. Mater. Interfaces*, 2017, **4**, 1600768.
110 J. Li, Q. Li, Y. Zeng, T. Tang, Y. Pan and L. Li, *RSC Adv.*, 2015, **5**, 717–725.
111 H. Mao, J. Liang, H. Zhang, Q. Pei, D. Liu, S. Wu, Y. Zhang and X. M. Song, *Biosens. Bioelectron.*, 2015, **70**, 289–298.
112 H. Kazerooni and B. Nassernejad, *RSC Adv.*, 2014, **4**, 34604–34609.
113 L. Cseri, J. Baugh, A. Alabi, A. AlHajaj, L. Zou, R. A. W. Dryfe, P. M. Budd and G. Szekely, *J. Mater. Chem. A*, 2018, **6**, 24728–24739.
114 H. He, S. Averick, E. Roth, D. Luebke, H. Nulwala and K. Matyjaszewski, *Polymer*, 2014, **55**, 3330–3338.
115 S. Wang, Q. X. Shi, Y. S. Ye, Y. Xue, Y. Wang, H. Y. Peng, X. L. Xie and Y. W. Mai, *Nano Energy*, 2017, **33**, 110–123.
116 X. Li, S. Li, Z. Zhang, J. Huang, L. Yang and S. Hirano, *J. Mater. Chem. A*, 2016, **4**, 13822–13829.
117 P. Wang, Y. N. Zhou, J. S. Luo and Z. H. Luo, *Polym. Chem.*, 2014, **5**, 882–891.
118 H. Cheng, P. Wang, J. Luo, J. Fransaer, D. E. De Vos and Z. H. Luo, *Ind. Eng. Chem. Res.*, 2015, **54**, 3107–3115.
119 H. Qiu, A. K. Mallik, M. Takafuji, S. Jiang and H. Ihara, *Analyst*, 2012, **137**, 2553–2555.
120 S. Badragheh, M. Zee and M. R. T. B. Olyai, *RSC Adv.*, 2018, **8**, 30550–30561.
121 W. Hou, Q. Wang, Z. Guo, J. Li, Y. Zhou and J. Wang, *Catal. Sci. Technol.*, 2017, **7**, 1006–1016.
122 G. Zarca, W. J. Horne, I. Ortiz, A. Urtiaga and J. E. Bara, *J. Membr. Sci.*, 2016, **515**, 109–114.
123 X. Sui, M. A. Hempenius and G. J. Vancso, *J. Am. Chem. Soc.*, 2012, **134**, 4023–4025.
124 X. Feng, K. Zhang, P. Chen, X. Sui, M. A. Hempenius, B. Liedberg and G. J. Vancso, *Macromol. Rapid Commun.*, 2016, **37**, 1939–1944.
125 K. Zhang, X. Feng, X. Sui, M. A. Hempenius and G. J. Vancso, *Angew. Chem., Int. Ed.*, 2014, **53**, 13789–13793.
126 X. Feng, X. Sui, M. A. Hempenius and G. J. Vancso, *J. Am. Chem. Soc.*, 2014, **136**, 7865–7868.
127 K. Zhang, M. Zhang, X. Feng, M. A. Hempenius and G. J. Vancso, *Adv. Funct. Mater.*, 2017, **27**, 1702784.
128 C. Yuan, J. Guo, M. Tan, M. Guo, L. Qiu and F. Yan, *ACS Macro Lett.*, 2014, **3**, 271–275.
129 J. Guo, C. Yuan, M. Guo, L. Wang and F. Yan, *Chem. Sci.*, 2014, **5**, 3261–3266.
130 S. Doherty, J. G. Knight, M. A. Carroll, A. R. Clemmet, J. R. Ellison, T. Backhouse, N. Holmes, L. A. Thompson and R. A. Bourne, *RSC Adv.*, 2016, **6**, 73118.
131 C. Gao, G. Chen, X. Wang, J. Li, Y. Zhou and J. Wang, *Chem. Commun.*, 2015, **51**, 4969–4972.
132 P. Zhao, Y. Leng and J. Wang, *Chem. Eng. J.*, 2012, **204–206**, 72–78.
133 G. Chen, W. Hou, J. Li, X. Wang, Y. Zhou and J. Wang, *Dalton Trans.*, 2016, **45**, 4504–4508.
134 Y. Leng, J. Wu, P. Jiang and J. Wang, *Catal. Sci. Technol.*, 2014, **4**, 1293–1300.
135 Y. Leng, J. Liu, P. Jiang and J. Wang, *ACS Sustainable Chem. Eng.*, 2015, **3**, 170–176.
136 N. N. Rozik and S. L. Abd El-Messieh, *Polym. Bull.*, 2017, **74**, 3595–3604.
137 M. Tokuda, T. Shindo and H. Minami, *Langmuir*, 2013, **29**, 11284–11289.
138 C. Zheng, Y. Liu, Y. Dong, F. He, X. Zhao and J. Yin, *Macromol. Rapid Commun.*, 2018, 1800351.
139 Q. Zhao, P. Zhang, M. Antonietti and J. Yuan, *J. Am. Chem. Soc.*, 2012, **134**, 11852–11855.
140 V. K. Tiwari, Y. Lee, G. Song, K. L. Kim, Y. J. Park and C. Park, *J. Polym. Sci., Part B: Polym. Phys.*, 2018, **56**, 795–802.
141 Y. Li, Y. Song, X. Zhang, X. Wu, F. Wang and Z. Wang, *Macromol. Chem. Phys.*, 2015, **216**, 113–121.
142 A. S. Rewar, H. D. Chaudhari, R. Illathvalappil, K. Sreekumar and U. K. Kharul, *J. Mater. Chem. A*, 2014, **2**, 14449–14458.
143 Y. Ren, J. Guo, Q. Lu, D. Xu, J. Qin and F. Yan, *ChemSusChem*, 2018, **11**, 1092–1098.
144 P. Y. Zheng, C. C. Ye, X. S. Wang, K. F. Chen, Q. F. An, K. R. Lee and C. J. Gao, *J. Membr. Sci.*, 2016, **510**, 220–228.
145 C. Yuan, J. Guo and F. Yan, *Polymer*, 2014, **55**, 3431–3435.
146 Z. Zhang, Q. Zhao, J. Yuan, M. Antonietti and F. Huang, *Chem. Commun.*, 2014, **50**, 595–2597.
147 S. Zhou, N. Song, X. Lv and Q. Jia, *J. Chromatogr. A*, 2018, **1565**, 19–28.
148 J. K. Sun, W. Zhang, R. Guterman, H. J. Lin and J. Yuan, *Nat. Commun.*, 2018, **9**, 1717.
149 T. Kitao, Y. Zhang, S. Kitagawa, B. Wang and T. Uemura, *Chem. Soc. Rev.*, 2017, **46**, 3108–3133.

 

150 J. Chen, M. Zhong, L. Tao, L. Liu, S. Jayakumar, C. Li, H. Li and Q. Yang, *Green Chem.*, 2018, **20**, 903–911.
151 Q. Sun, B. Aguila, J. Perman, N. Nguyen and S. Ma, *J. Am. Chem. Soc.*, 2016, **138**, 15790–15796.
152 W. Wang, C. Li, L. Yan, Y. Wang, M. Jiang and Y. Ding, *ACS Catal.*, 2016, **6**, 6091–6100.
153 M. Ding and H.-L. Jiang, *ACS Catal.*, 2018, **8**, 3194–3201.
154 Q. Guo, C. Chen, L. Zhou, X. Lia, Z. Li, D. Yuan, J. Ding, H. Wan and G. Guan, *Microporous Mesoporous Mater.*, 2018, **261**, 79–87.
155 L. Hao, P. Li, T. Yang and T. S. Chung, *J. Membr. Sci.*, 2013, **436**, 221–231.
156 A. R. Nabais, A. P. S. Martins, V. D. Alves, J. G. Crespo, I. M. Marrucho, L. C. Tomé and L. A. Neves, *Sep. Purif. Technol.*, 2019, **222**, 168–176.
157 J. F. Olorunyomi, K. Y. Chan, L. Gao and C. Y. V. Li, *Microporous Mesoporous Mater.*, 2018, **259**, 255–263.
158 L. Gao, C. Ying, V. Li, K. Y. Chan and Z. N. Chen, *J. Am. Chem. Soc.*, 2014, **136**, 7209–7212.
159 M. Isik, T. Lonjaret, H. Sardon, R. Marcilla, T. Herve, G. G. Malliaras, E. Ismailova and D. Mecerreyes, *J. Mater. Chem. C*, 2015, **3**, 8942–8948.
160 M. Isik, R. Gracia, L. C. Kollnus, L. C. Tomé, I. M. Marrucho and D. Mecerreyes, *ACS Macro Lett.*, 2013, **2**, 1975–1979.
161 K. Grygiel, B. Wicklein, Q. Zhao, M. Eder, T. Pettersson, L. Bergström, M. Antoniettia and J. Yuan, *Chem. Commun.*, 2014, **50**, 12486–12489.
162 B. Zhang, G. Sudre, G. Quintard, A. Serghei, L. David, J. Bernard, E. Fleury and A. Charlot, *Carbohydr. Polym.*, 2017, **157**, 586–595.
163 P. Zhang, J. Yuan, T. P. Fellinger, M. Antonietti, H. Li and Y. Wang, *Angew. Chem., Int. Ed.*, 2013, **52**, 6028–6032.
164 W. Zhang, H. Shimakoshi, N. Houfuku, X. M. Song and Y. Hisaeda, *Dalton Trans.*, 2014, **43**, 13972–13978.
165 K. Nakashima, N. Kamiya, D. Koda, T. Maruyamac and M. Goto, *Org. Biomol. Chem.*, 2009, **7**, 2353–2358.
166 A. Grollmisch, U. Kragl and J. Großeheilmann, *SynOpen*, 2018, **2**, 192–199.
167 K. Manojkumar, K. T. Prabhu Charan, A. Sivaramakrishna, P. C. Jha, V. M. Khedkar, R. Siva, G. Jayaraman and K. Vijayakrishna, *Biomacromolecules*, 2015, **16**, 894–903.
168 J. L. Freyer, S. D. Brucks, G. S. Gobieski, S. T. Russell, C. E. Yozwiak, M. Sun, Z. Chen, Y. Jiang, J. S. Bandar, B. R. Stockwell, T. H. Lambert and L. M. Campos, *Angew. Chem., Int. Ed.*, 2016, **55**, 12382–12386.
169 H. Zhang, C. Liu, L. Zheng, W. Feng, Z. Zhou and J. Nie, *Electrochim. Acta*, 2015, **159**, 93–101.
170 J. Yuan and M. Antonietti, *Macromolecules*, 2011, **44**, 744–750.
171 J. Zamory, M. Bedu, S. Fantini, S. Passerini and E. Paillard, *J. Power Sources*, 2013, **240**, 745–752.
172 A. Vizintin, R. Guterman, J. Schmidt, M. Antonietti and R. Dominko, *Chem. Mater.*, 2018, **30**, 5444–5450.
173 L. Li, T. A. Pascal, J. G. Connell, F. Y. Fan, S. M. Meckler, L. Ma, Y. M. Chiang, D. Prendergast and B. A. Helms, *Nat. Commun.*, 2017, **8**, 2277.
174 Y. S. Ye, J. Rick and B. J. Hwang, *J. Mater. Chem. A*, 2013, **1**, 2719–2743.
175 J. Le Bideau, L. Viau and A. Vioux, *Chem. Soc. Rev.*, 2011, **40**, 907–925.
176 M. G. Cowan, A. M. Lopez, M. Masuda, Y. Kohno, W. M. McDanel, R. D. Noble and D. L. Gin, *Macromol. Rapid Commun.*, 2016, **37**, 1150–1154.
177 P. H. Wang, T. L. Wang, W. C. Lin, H. Y. Lin, M. H. Lee and C. H. Yang, *Nanomaterials*, 2018, **8**, 225.
178 P. S. C. de Oliveira, S. A. Alexandre, G. G. Silva, J. P. C. Trigueiro and R. L. Lavall, *Eur. Polym. J.*, 2018, **108**, 452–460.
179 M. G. Cowan, D. L. Gin and R. D. Noble, *Acc. Chem. Res.*, 2016, **49**, 724–732.
180 D. L. Gin and R. D. Noble, *Science*, 2011, **332**, 674–676.
181 Z. Dai, R. D. Noble, D. L. Gin, X. Zhang and L. Deng, *J. Membr. Sci.*, 2016, **497**, 1–20.
182 L. C. Tomé and I. M. Marrucho, *Chem. Soc. Rev.*, 2016, **45**, 2785–2824.
183 L. C. Tomé, D. Mecerreyes, C. S. R. Freire, L. P. N. Rebel and I. M. Marrucho, *J. Membr. Sci.*, 2013, **428**, 260–266.
184 J. E. Bara, E. S. Hatakeyama, D. L. Gin and R. D. Noble, *Polym. Adv. Technol.*, 2008, **19**, 1415–1420.
185 P. Li, K. P. Pramoda and T. S. Chung, *Ind. Eng. Chem. Res.*, 2011, **50**, 9344–9353.
186 T. K. Carlisle, G. D. Nicodemus, D. L. Gin and R. D. Noble, *J. Membr. Sci.*, 2012, **397–398**, 24–37.
187 S. V. Shaligram, P. P. Wadgaonkar and U. K. Kharul, *J. Membr. Sci.*, 2015, **493**, 403–413.
188 A. S. L. Gouveia, L. Ventaja, L. C. Tomé and I. M. Marrucho, *Membranes*, 2018, **8**, 124.
189 M. Ambrogi, K. Täuber, M. Antonietti and J. Yuan, *J. Mater. Chem. A*, 2015, **3**, 5778–5782.
190 R. O. Mäkiniemi, P. Das, D. Hönders, K. Grygiel, D. Cordella, C. Detrembleur, J. Yuan and A. Walther, *ACS Appl. Mater. Interfaces*, 2015, **7**, 15681–15685.
191 G. Hernández, M. Işik, D. Mantione, A. Pendashteh, P. Navalpotro, D. Shanmukaraj, R. Marcilla and D. Mecerreyes, *J. Mater. Chem. A*, 2017, **5**, 16231–16240.
192 D. Wu, Y. Yu, J. Zhang, L. Guo and Y. Kong, *ACS Appl. Mater. Interfaces*, 2018, **10**, 23362–23368.
193 N. Pothanagandhi, A. Sivaramakrishna and K. Vijayakrishna, *Polym. Chem.*, 2017, **8**, 918–925.